Dating of alluvial fans from NW Argentina using cosmogenic nuclides and optically stimulated luminescence technique

MASTERTHESIS

Submitted on

19.06.2018

by

Carolin Reger

Prüfungskomission:

1. Advisor: Prof. Dr. Manfred R. Strecker (Universität Potsdam)
2. Advisor: Dr. Paolo Ballato (Universität Potsdam)

Tag der Disputation: 19. June 2018

Published online in the
Institutional Repository of the University of Potsdam:
https://doi.org/10.25932/publishup-47147
https://nbn-resolving.org/urn:nbn:de:kobv:517-opus4-471470

Table of contents

Table of figures

Abstract

Alluvial fans are important geomorphic markers and sedimentary archives of tectonic and climatic changes. Hence, basins providing perfect studying conditions can often be found in arid regions due to the low weathering impact and thus well preservation of sedimentary features. Twelve samples for optically/infrared stimulated luminescence (OSL/IRSL) dating and one depth profile for cosmogenic radionuclide dating (^{10}Be) were collected in the Santa Maria Valley in NW Argentina, where the exceptional preservation of several generations of alluvial fans allow exploring the external forcing conditions that led to repeated cycles of incision and aggradation. The results of the OSL/IRSL dating yielded ages ranging between 0.4 ± 0.1 ka and 271.8 ± 24.5 ka. Previous studies next to the study area indicate a depositional age of 1.5-2 Mio years for the oldest generation of alluvial fans, which might still be supported by our ongoing ^{10}Be dating. Due to field observations, sediment provenance, stratigraphic characteristics and the geomorphic pattern of erosion, seven (/eight) generations of alluvial fan deposits were recognized. Comparing my ages with global glaciation cycles as well as linking them to temperature proxies retrieved from a lake on the Altiplano Plateau, a good fit between alluvial fan accumulation phases and global glacial periods (corresponding to cold/wet phases within the central Andes) is observed. This suggests that aggradation occurs during the early stages of glacial periods, while incision is expected at the end of glacial phases. This pattern might be linked to variations in the vegetational cover (controlled by water availability), which will decrease/increase during hot and dry/cold and wet interglacial/glacial phases favoring/limiting sediment production and will increase/decrease during cold and wet/hot and dry glacial/interglacial phases. Even though the eastern Andean margin is showing neotectonic activities and is assumed to be active up to recent times, deformation and seismicity might most probably have played only a minor role in relation to the rather short timescale reflected by the data.

Zusammenfassung

Schwemmfächer stellen wichtige geomorphologische Erkennungszeichen und gute sedimentologische Archive von tektonischen wie auch klimatischen Veränderungen dar. Aus diesem Grund sind Becken mit ausgezeichneten Forschungsbedingungen oft in ariden Gebieten vorzufinden, da die Schwemmfächer auf Grund der geringen Verwitterung in diesen Gebieten meist gut erhalten sind. Im Santa Maria Tal in NW Argentinien wurden zwölf Proben zur Datierung mit Optisch/Infrarot Stimulierter Lumineszenz (OSL/IRSL) genommen sowie ein Tiefenprofil zur Datierung des kosmogenen Radionuklids ^{10}Be erstellt. Die gute Erhaltung mehrerer Generationen von Schwemmfächern in diesem Gebiet gestattet die Untersuchung externer Bedingungen, welche zu wiederholten Zyklen von Akkumulation und Einschneidung der alluvialen Ablagerungen führten. Die Ergebnisse der OSL/IRSL Datierung lieferten Alter zwischen 0.4 ± 0.1 ka und 271.8 ± 24.5 ka. Frühere Veröffentlichungen zu angrenzenden Forschungsgebieten ließen auf ein maximales Alter der ältesten Schwemmfächer-Generation von 1.5-2 Millionen Jahren schließen, was in Zukunft noch durch die laufenden ^{10}Be-Datierungen belegt werden könnte. Sieben (/acht) Generationen von Schwemmfächern konnten, gestützt durch die Altersdatierungen sowie Geländebeobachtungen zu Herkunft der Sedimente, stratigraphische Eigenschaften und Beobachtungen zum geomorphologischen Erosionsmuster des jeweiligen Schwemmfächers, unterschieden werden. Bei dem Vergleich meiner Daten mit globalen glazialen Zyklen sowie einem Temperatur-Proxy aus einem Seebohrkern auf dem Altiplano-Plateau, überschnitten sich die Ablagerungsphasen der Schwemmfächer im Santa Maria Becken mit globalen Kaltzeiten und kalten/feuchten Zyklen innerhalb der Anden. Es besteht die Annahme, dass Ablagerung während dem Übergang von Warm- zu Kaltzeiten bis hin zu glazialen Maxima auftritt, während Phasen der Einschneidung gegen Ende globaler Kaltzeiten zu erwarten sind. Dieses Muster dürfte durch die Varianz an Vegetationsbedeckung, bedingt durch die klimatischen Schwankungen, zu erklären sein, welche wahrscheinlich bei erhöhter Dichte (Kaltzeiten) als Sedimentbarriere an der Grenze der Sediment-Ursprungsregion dient. Trotz der in der Vergangenheit auftretenden, neotektonischen Aktivitäten am östlichen Rand der Anden und der Annahme anhaltender tektonischer Aktivität wird Deformation und seismischen Aktivitäten auf

Grund der kurzen Zeitspanne, welche von den Daten umfasst wird, nur eine Nebenrolle im Entstehungsprozess der Schwemmfächer zugeschrieben.

1. Introduction

In 2015 the United Nations Framework Convention on Climate Change (UNFCCC) set up the Paris climate agreement which was signed by almost 200 nations. Within this document the participating parties agreed on a mitigation of the greenhouse gas emission to prevent a global temperature increase of 1.5°C (compared to pre-industrialisation) by 2040. Recently the International Panel on Climate Change (IPCC) published a paper (Millar et al., 2017), stating that the set aim of the UNFCCC members to stay below the 1.5°C limit might be very unlikely due to the prolonged emission of greenhouse gases.

In the face of the political attempts to get control over the process of global warming, geoscientists all over the world have been trying to estimate the effects of climate change on landscape evolution, which results from a combination of surface and tectonic processes. Hence there is a need for a deeper understanding of the interplay between the Earth and the atmosphere, geomorphological processes and climate. Many studies proposed the occurrence of feedbacks between mountain uplift and erosion, which is primarily controlled by climate, due to erosional unloading and redistribution of sediments in adjacent basins within tectonically active regions (e.g. Molnar & England, 1990; Willett, 1999; Sobel et al., 2003; Whipple & Meade, 2006; Whipple, 2009). This leads to the assumption that an increase in precipitation results in a higher erosional flux and therefore more mass unloading and ultimately an increase in sedimentation rates. Due to the lithostatic rebound effect surface uplift occurs, which would lead to (further) climatic shielding by mountain ranges of adjacent basins of wind and precipitation. Thus, mass wasting and sediment accumulation is restricted to the shielded, leeward basins. The weight of the trapped sediments in the basins causes lithostatic stress and therefore might induce faults propagating to undeformed regions in the foreland areas. In general, this would indicate a growth of the mountainous area in leeward direction, which was already suggested e.g. by Sobel et al. (2003). As an example, this model was proposed for the Himalayas (Hodges, 2000; Thiede et al., 2005), Taiwan (e.g. Dadson et al., 2003) and tested with several models (e.g. Stolar et al., 2007). Similar observations were made in the South American Andes, particularly in the Subandean foreland of the

Central Andes (15-34°S). Several studies have been taken out within this area of outstanding changes of regional climate linked to the local morphology with high mountain chains neighbouring deep valleys. These valleys serve as sediment sinks and provide excellent datable material for studies concerning the interplay between surface processes (which are primarily controlled by climate) and tectonics. Here, geomorphic markers come into play, which are “identifiable geomorphic features or surfaces that provide a reference frame against which to gauge differential or absolute deformation” (Burbank & Anderson, 2001). Three characteristics should be given for dating considerations: 1) Good preservation, 2) a consistent geometry and 3) a supposed age range of the given features, which matches the requirements of the study. One of these geomorphic markers are alluvial fans. They occur mostly in regions of high topography when sediments are transported downhill, either by fluvial or gravity-driven processes, and deposited in topographic depressions, where they can represent massive thick and extensive sedimentary bodies.

Alluvial fan surfaces are geomorphically comparable to river longitudinal profiles and consequently river terraces and exhibit a down-fan decrease of slope as well as a concave upward profile (Burbank & Anderson, 2001). They can be recognised by their characteristic shape, which was described by Bull (1977) and Blair & McPherson (1994) to “resemble the segment of a cone radiating downslope from a point where a channel emerges from an upland”. The depositional process of alluvial fans depends on sediment supply as well as on water availability. They consist of clastic material of variable grain size depending on the source rock type, erosional and depositional processes. Based on the energy of the flooding event even bigger blocks could be embedded in single units. Depending on water saturation, stream energy and the shape of the clasts, imbrication can occur, indicating the flow direction of the paleostream. In many cases a distinct bedding can be observed alongside the fan, which is mostly defined by vertical size-sorting of the clasts. In many cases, alluvial fans show cementation, based on the given local climatic conditions and the matrix material as well as their age. The stratigraphic characteristics of alluvial fans can directly be linked to the local geology, tectonics and climate. Climatically, humid systems with a well-developed stream network differentiate from rather dry regions, where irregular periods of high precipitation would provide the main source of erosional energy and transport capacity. In case of

arid regions and depending on the basin size and material availability, several fan generations often occur in a “telescopic” kind of depositional structure (Blair & McPherson, 2009), where older fans are incised by younger fan generations, eroding old fan material and depositing new material at the foot of the old fan generation. Fans within arid regions are preferably being studied due to their good preservation, excellent exposure and ease of access (Blair & McPherson, 1994; Blair & McPherson, 2009).

Such an area of arid alluvial fan occurrence can be found in the eastern foreland of the Andes from the Puna Plateau to the Eastern Cordillera and the Santa Barbara System. Within this area, a set of alluvial fans can be observed, which tend to differ in their height and depositional ages from first observations using aerial photographs. This automatically leads to the assumption, that single phases of deposition were triggered by specific conditions, alternating with periods of incision.

The Santa Barbara system and the Calchaquí Basin provide well preserved strata to study the deposition of alluvial fans and their controlling factors. To understand the feedback mechanisms between tectonics and climate, we need a deeper understanding of the geometry, sedimentological characteristics and the chronology of alluvial fans. Thus, the major aim of this thesis is to understand what processes controlled the alternation between periods of aggradation and incision. I tried to achieve this by taking samples from 10 locations, belonging to different fans and date them using optically stimulated luminescence (OSL) and cosmogenic radionuclide surface dating for the highest alluvial fans. The obtained dates were then linked up with data from regional climate archives for the specific periods to sustain a deeper understanding of the interplay between climate and phases of aggradation/incision.

Similar observations were made in previous studies, for example by Dey et al. (2016) in the Kangra basin (northwestern Sub-Himalaya), where cosmogenic nuclide (^{10}Be) and OSL were used to date different fans. They concluded that the accumulation of alluvial terraces was influenced by periods of intensified Indian Summer Monsoon as well as glacial retreat from the last interglacial (which increased the sediment input), based on a correlation between their ages, which documented alluvial fan abandonment, and regional paleoclimatic proxies. Incision again, occurred during periods of low Indian Summer Monsoon and reduced sediment flux.

Another study by Tofelde et al. (2017) was taken out in the Toro Basin, where five generations of fluvial terraces cut into two alluvial fans were studied by surface exposure dating with cosmogenic nuclide (^{10}Be) depth profiles. Additionally depositional ages determined by ^{26}Al/^{10}Be burial samples and U-Pb zircon ages of ash samples were processed. They observed a 100 kyr cycle of fill and incisional phases whereas incision occurred during wet and cold (global glacial maxima/wet conditions on the Altiplano) and enhanced deposition during dry and warmer phases (global interglacials/dry conditions on the Altiplano). They explained this observation with eccentricity-driven climate change.

This thesis is associated with the thesis of Sophie Boven, where stratigraphic and cross cutting relationships are used in combination with the results of this thesis to detect the chronology of major Quaternary deformation events.

2. Geological and climatic setting

2.1. Introduction of the Southern-Central Andes

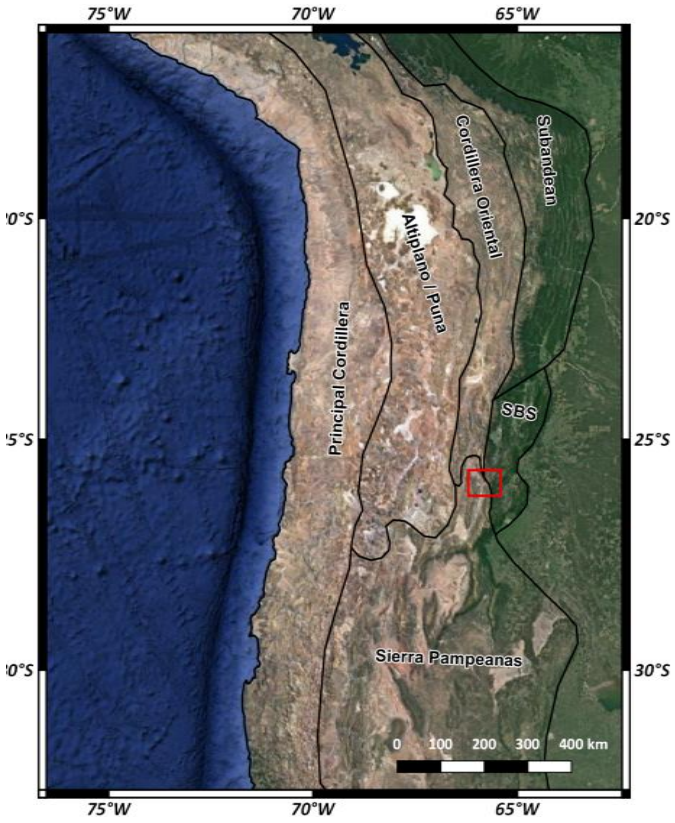

Figure 1 – Overview of the morphotectonic provinces of the Southern-Central Andes. The location of the study area is marked by a red box.

(Basemap from Google Earth, 2018)

Parallel to the western coast of South-America, the largest non-collisional orogen on earth can be found – the Andes. This mountain range has an approximate length of 7000 km and peak heights of more than six kilometres. Due to both their latitudinal and altitudinal size the Andes influence regional climate and occupy different climatic zones (e.g. Strecker et al., 2007).

The Andes are located at a plate convergence margin, where the Nazca oceanic plate, and partly the Antarctic plate at the latitude of the Pantagonean Andes, subduct underneath the South-American plate. Importantly, slab angle variations of the Nazca plate, are thought to have shaped the whole orogen. Within the latitudinal sections of 2-15°S and 27-33°S, the Benioff zone has a dip of 5-10° east whereas in the section of 15-24°S, it exhibits a dip angle of up to 30° east (Jordan et al., 1983).

Due to the location of the study area, the focus of this thesis remains on the southern-central section of the Andes, which stretches from 15°S to 33°S and can be subdivided in several morphotectonic provinces (see figure 1). In the very western section, the Principal Western Cordillera stretches along the coast with a coast-parallel volcanic axis. Active volcanism only occurs within the steep slab section of 15-24°S. East of the Principal Cordillera the adjacent Puna-Altiplano Plateau can be

found, the second largest orogenic plateau on Earth, with maximum longitudinal extension of 1800km, a width of 350-400 km and basin elevations of 3.7 to 4.4 km (Allmedinger et al., 1997, Jordan et al., 1983, Jordan et. al, 2010). The north-eastern border of the Altiplano-Puna Plateau is being represented by the Eastern Cordillera, a thick skinned, north-northeast striking orogen including thrust and high angle reverse fault systems deforming Paleozoic to Miocene rocks. This sector of the Andes also contains multiple deeply eroded alluvial fans, documenting active tectonics (Allmendinger et al., 1983). The neighbouring Subandean foreland comprises continuous lateral folds and west-dipping listric thrust faults rooting at depth with a regional detachment horizon (e.g. McQuarrie et al., 2005).

The previously mentioned flat-angled slab area of 27-33°S comprises the Sierras Pampeanas and the Santa Barbara System (SBS), which are also representing the (seismic) transition zone to the southern section of the Andes. The Sierras Pampeanas are a broad section of uplifted Precambrian to Paleozoic crystalline basement blocks with 2-6 km of elevation, 75-100 km length and maximum width of up to 75 km (Allmendinger et al., 1983; Jordan et al., 1983; Strecker et al., 1989; Strecker et al., 2007). The single blocks were uplifted along north-northwest south-southeast trending inward dipping reverse faults with maximum dips of 60° and are separated by wide basins with average base elevations of 1 km.

The Santa Barbara System (SBS), a former rift basin of Cretaceous age, comprises large asymmetric folds and west-verging faults, which are not laterally continuous like in the Subandean foreland to the north. Strata of up to Precambrian age is being exposed in the cores of the anticlines. The major faults within the basin are steeply dipping reverse faults of Cretaceous age, which were partly reactivated in the Miocene and might be active until today (Allmendinger et al., 1983; Jordan et al., 1983, Strecker et al., 2007).

2.2. Physiography and stratigraphic units of the study area

The study area is located at the transition zone between the Sierras Pampeanas and the Santa Barbara System. It consists of basement blocks of the Sierra de Quilmes, Sierra Cumbres Calchaquíes and the Sierra Aconquija that bound the Santa María Valley (see figure 2 and 3). These blocks were uplifted along high-angle reverse faults, which are obliquely oriented with respect to the late Cenozoic northwest-southeast to west-northwest east-southeast shortening direction (Hermanns & Strecker, 1999; Carrera et al., 2006). These basement rocks include the Puncoviscana Formation, which mainly consists of metamorphically imprinted thin beds of sandstones and shales of Precambrian to Lower Cambrian age and minor amounts of Ordovician pelites (Carrera et al., 2006). The Cumbres Calchaquíes are fault bounded to the east and the west; the Sierra Aconquija is fault-bounded only to the west and the Sierra de Quilmes, which is part

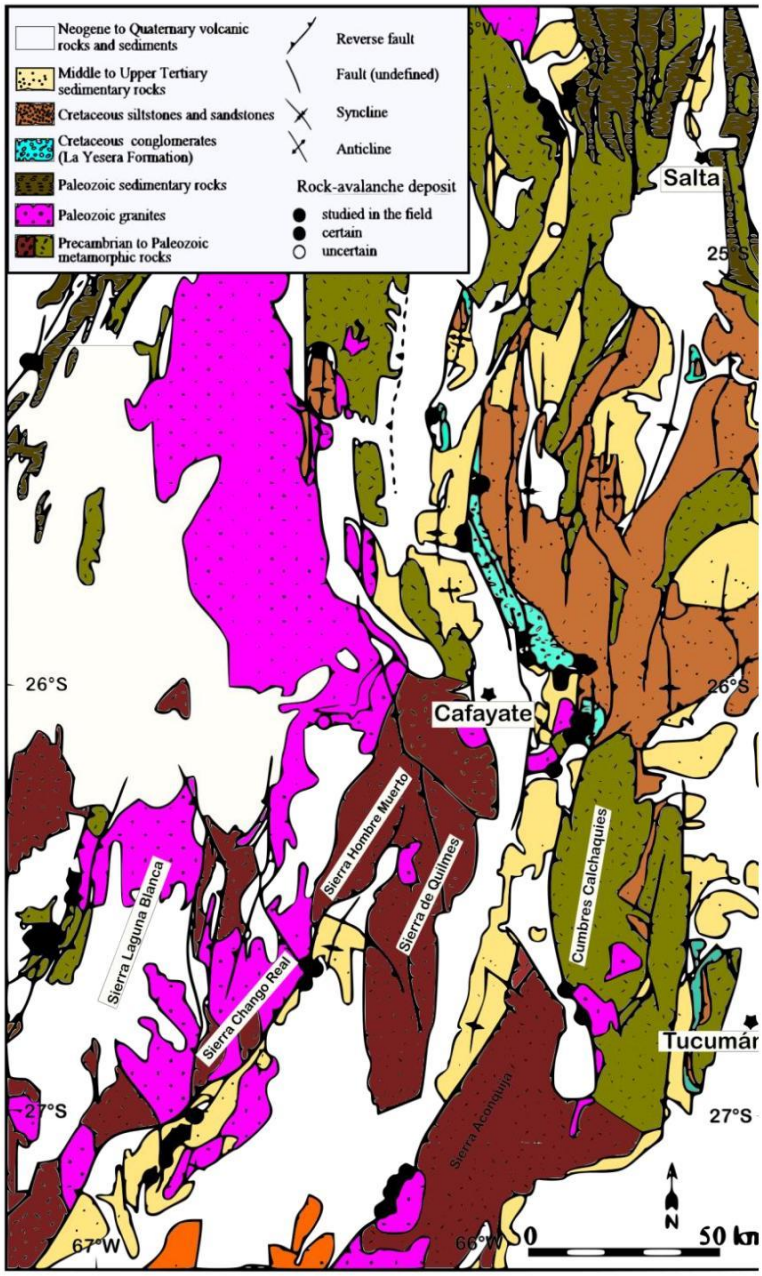

Figure 2 – Simplified geologic map of the central Andes including the study area, marked by the yellow box.

Modified after Hermanns & Strecker (1999) and Sobel & Strecker (2003).

of the morphotectonic transitional zone at the eastern margin of the Puna plateau, is fault-bounded on both sides of the range.

The study area partly belongs to the nationalpark Quebrada de las Conchas, which is the area around the valley of the Río de las Conchas, connecting the Lerma valley with the Calchaquíes valley.

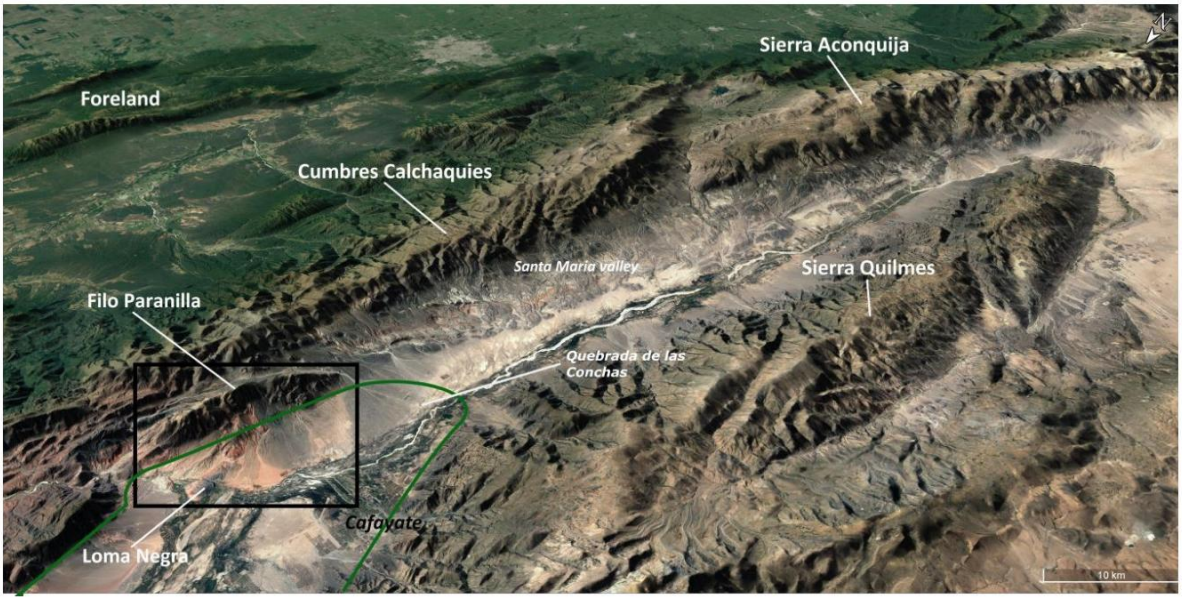

Figure 3 – Southeast-ward overview of the Santa Maria Valley. The Cumbres Calchaquies, Sierra Quilmes and Sierra Aconquija are the most distinctive mountain ranges limiting the Puna Plateau in the northwest and the Santa Maria valley itself. The black box marks the study area, the green line shows the location of the Quebrada de las Conchas.

(Google Earth, 2018)

The small mountain range called Filo Paranilla dominating the morphology of the study area is located in the east of the Quebrada de las Conchas and part of the Sierra Cumbres Calchaquíes (see figure 3). It is an anticlinal structure, which is fault bounded to the east by a west verging thrust-fault. The most prominent fault within the region, which is also connected to most seismic activity is the El-Zorrito-Las-Chacras thrust fault, east of the Filo Paranilla, at the margin of the Cumbres Calchaquíes (Carrera et al., 2006). Stratigraphically, the Filo Paranilla comprises three areas - two with granitic rocks in its northern and southern sectors and metamorphic rocks (mostly biotite schist) in the middle part (see figure 22, Appendix). The granite is rich in quartz and K-feldspar, rather low in biotite and shows, due to the K-feldspar, a distinct reddish colouring. The study area includes apart from the Filo Paranilla another, smaller anticline in the northwest, the Loma Negra. This small

rise consists mainly of schists (like the central part of the Filo Paranilla) and was incised by the Río de las Conchas. The basin in between those two anticlines partly shows structures linked to deformation (Grier et al., 1991; Carrera et al., 2006).

Regarding the stratigraphy of the Southern Sierras Pampeanas region (Fig. 4), the Puncoviscana basement is discordantly covered by Cretaceous deposits due to the absence of Paleozoic material (apart from granitic intrusions). Within the Santa Maria Basin we cannot observe any Cretaceous deposits, but they can be found more to the east, at the eastern flank of the Cumbres Calchaquíes (Sobel & Strecker, 2003; Carrera et al., 2006). The Cretaceous rift phase caused the deformation of the Salta Basin with several subbasins around the central uplifted Salta-Jujuy high and is reflected in syntectonic sediments defining the Salta Group (Carrera et al., 2006); the Study area is located in the Alemanía Basin, a sub-basin within the Salta Basin.

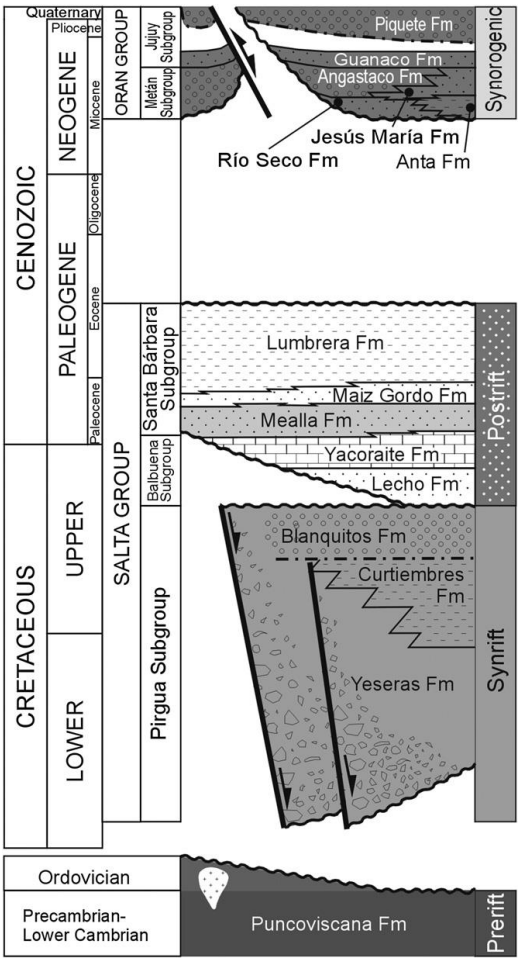

Figure 4 – Chronostratigraphic diagram linking the main units of the area with the most important tectonic events (Carrera et al., 2006).

The Pirgua Subgroup is the lowest member of the Salta Group and consists of alluvial and fluvial/marine material, interbedded with volcanic material with an alkaline geochemical signature.

The Pirgua Subgroup is unconformably covered by the Balbuena Subgroup (upper Cretaceous to early Paleocene) and the Santa Bárbara Subgroup (Paleocene to Mid-Eocene time). The latter can be found within the study area and consists of three fluvial/lacustrine formations: The Mealla, Maiz Gordo and Lumbrera formations. The Mealla Formation forms the lowest member of the Santa Bárbara Subgroup and consists mainly of fining upwards reddish sandstone, interbedded with massive reddish siltstone (Marquillas et al., 2005). This unit is covered by the Maiz Gordo Formation, which can be

subdivided in the eastern part of the Alemanía Basin into three sections: the lowest section with red, thick, massive siltstone and subordinate centimetric-thick sandstone beds; the middle one with fine-to medium-grained sandstone, massive laminated siltstone and on top “discrete laminar to low-relief domal stromatolites” (only in the Alemanía Basin); the top section with green shales, mudstones and wave-rippled grainstones (Marquillas et al., 2005).

Unconformably above the Maiz Gordo, the Lumbrera deposits form the uppermost unit of the Santa Bárbara Subgroup. The Lumbrera Formation can also be subdivided in three units: the lowest one consists of red, cross laminated and rippled sandstones and siltstones; the middle section, also known as the “Faja Verde”, is composed of dark green to grayish claystones and tabular, fine-grained sandstones and stromatolites; the uppermost section is composed of massive red siltstones and mudstones (Marquillas et al., 2005).

Paleoenvironmentally these facies were created in previously existing lacustrine environments in the centre of the basin and fluvial river systems in the outer zone. More or less energetic river structures were leading to lacustrine phases with fine lake deposits, which mostly show greenish colours. The uppermost Lumbrera section consists of silt- and mudstones, which can also be related to a low energetic lacustrine environment (Marquillas et al., 2005; Carrera et al., 2006).

These Paleogene sedimentary units are conformably covered by Neogene sediments, recording the transition from foreland to intermontane basins as proposed by several studies (e.g. Hain et al., 2011; Strecker et al., 2011). There, deposition occurred in alluvial fan settings and braided river systems and provide evidence for tectonic activity at least since the late Pliocene (Grier et al., 1991; Hermanns & Strecker, 1999). They mainly consist of sandy material (in the southern Sierra Pampeanas rather coarse but fining northward) and conglomerates originating from the uplifted Puncoviscana basement and granitic intrusion blocks. Same accounts for the study area, where Puncoviscana was uplifted in form of the Filo Paranilla and the Loma Negra. The alluvial fans within the area are mainly made up of granitic material as well as partly metamorphic clasts and show imbrication and coarse stratification. The supposed start of alluvial fan accumulation in the intermontane Santa Maria Valley was around 1.5-2 Ma due to apatite fission track dating of interlayered

volcanic ashes (Strecker et al.,1989). In particular, Strecker et al. (1989) recognized five generations of locally deformed alluvial fans south of the study area at the northern-western edge of the Sierra Aconquija, documenting repeated phases of aggradation and incision. The oldest age estimation may also apply to the oldest alluvial fan generation of the study area (fan 1); such an age will be hopefully supported by my ongoing cosmogenic nuclide dating (see section 3.3).

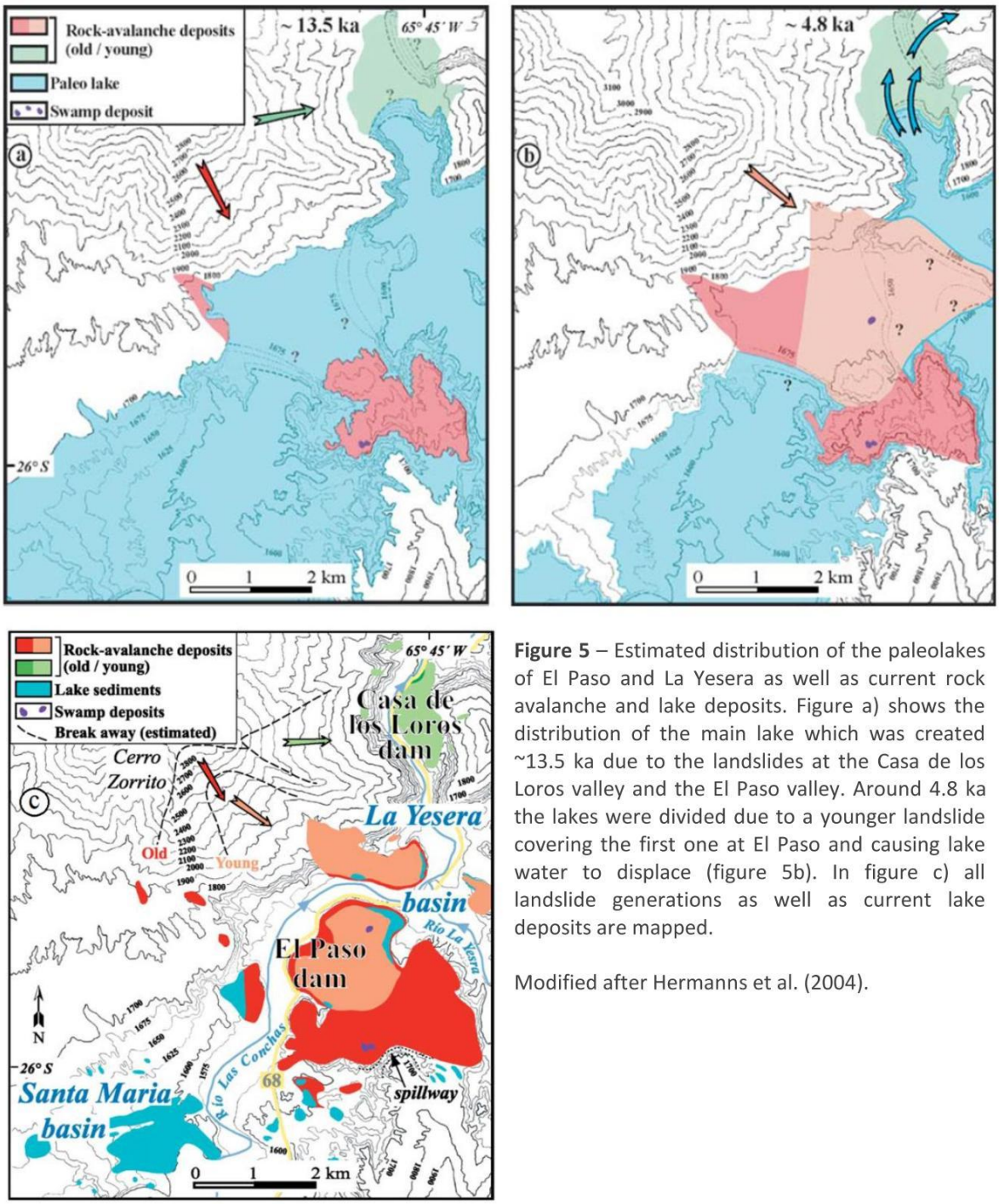

Figure 5 – Estimated distribution of the paleolakes of El Paso and La Yesera as well as current rock avalanche and lake deposits. Figure a) shows the distribution of the main lake which was created ~13.5 ka due to the landslides at the Casa de los Loros valley and the El Paso valley. Around 4.8 ka the lakes were divided due to a younger landslide covering the first one at El Paso and causing lake water to displace (figure 5b). In figure c) all landslide generations as well as current lake deposits are mapped.

Modified after Hermanns et al. (2004).

The youngest notable depositions within the study area are a set of lake deposits connected to several rock avalanches (Trauth & Strecker, 1999; Bookhagen et al., 2001; Hermanns et al., 2004; Hermanns et al., 2006). The first set of landslides occurred around 15.3 ± 2 ka and 13.55 ± 0.9 ka at the El Paso Valley and the Case de los Loros Valley, damming the Santa Maria and Yesera Basins and led to the development of one big lake (see figure 5a). This lake prevailed another avalanche around 7.5 ka until one major landslide occurred at 4.8 ± 0.5 ka, partly covering the old rock avalanche at El Paso and displacing big amounts of water. This led to the separation of the lake (see figure 5b). Figure 5c provides a compilation of the area today, showing residuals of the different landslides and lake deposits.

During the remote sensing stage of this thesis and the field work, these paleolake deposits stood out due to their light colouring. Looking at the contact between the alluvial fans and lake deposits, we observed onlapping of lake strata onto older alluvial fan deposits. Thus we concluded that the fans must be older than the lake deposits. Regardless, there might have been effects on the fan connectivity due to material removal by the lake (see chapter 5.2.).

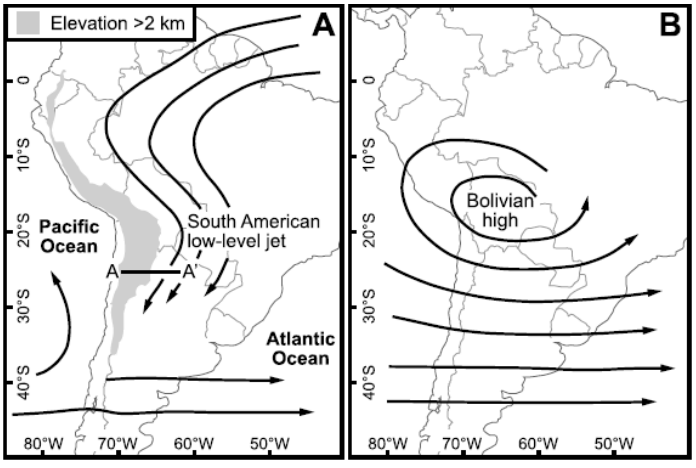

Figure 6 – Generalized patterns of South American atmospheric circulation during December-February.

(modified from Pingel et al., 2016)

2.3. Regional Climate

Within the area of the Southern-Central Andes several atmospheric circulation patterns exist and influence one another. One of the most prominent wind systems is represented by the westerlies (from 30-32°S to ca. 60°S), which trigger precipitation along the western flank of the Western Cordillera and transport hot, dry air as they cross the Andes to the interior of South America (figure 6B; Fiorella et al., 2015; Pingel et al., 2016).

The third component of the regional climatic pattern includes the easterly winds and the associated South American Monsoon, which transports moist air masses from the Atlantic over the Amazon Basin. As they reach the eastern flanks of the Andean orogen, they are deflected and flow southwards until ca. 30°S latitude (see figure 6A). This wind system is the so called South American low-level jet, and is responsible for sustained seasonal precipitation in the Eastern Andean foreland and the Eastern Cordillera (Pingel et al., 2016).

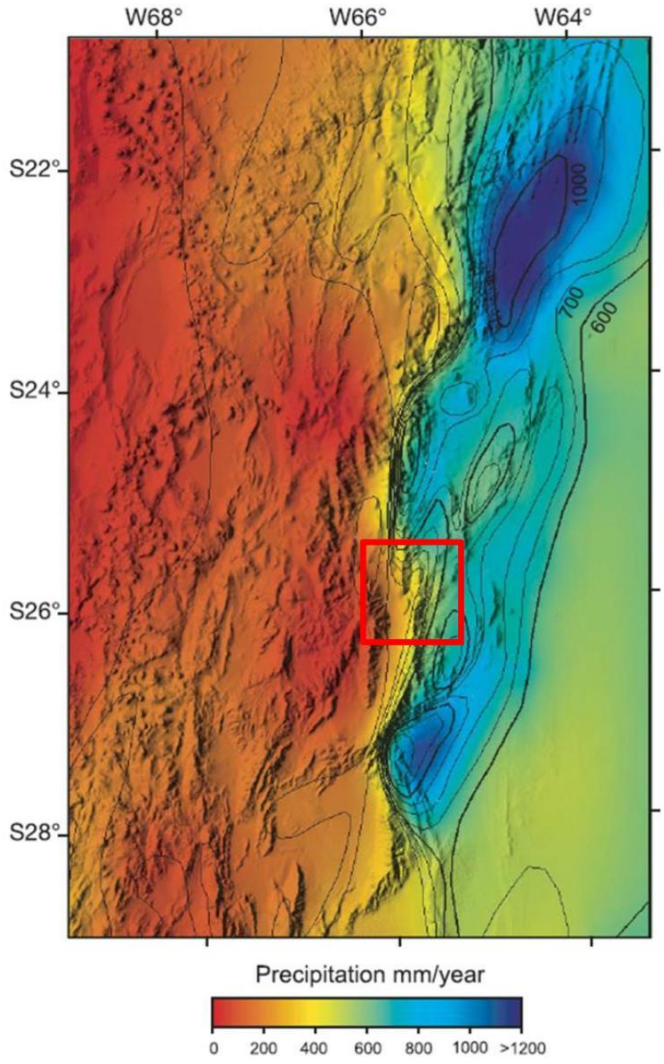

Figure 7 – Mean annual rainfall distribution over NW Argentina with contour lines. The red box shows the location of the study area.

(modified after Hilley & Strecker, 2005)

The central Andes are characterized by a steep gradient of precipitation values from 1300 mm/yr along the Eastern Cordillera and Sierra Pampeanas and less than 200 mm/yr in the interior of the Andean orogen (Fiorella et al., 2015; Pingel et al., 2016). The amount of annual precipitation is widely influenced by the strength and position of the Bolivian High (specifically precipitation within the Altiplano-Puna) as well as the state of the El Niño-Southern-Oscillation (Fiorella et al., 2015). The study area is located at the climatic margin of the dry regions of the Andes and counts as semiarid with an mean annual precipitation of 200-400 mm/yr (figure 7). Most of the rainfall appears during the wet summer seasons, while in winter only small amounts of precipitation are recorded. The reason for this sharp transition in precipitation is represented by high

topography along the easternmost ranges of the Cordillera Oriental/Sierras Pampeanas, which prevent the penetration of moist air masses of the South-American low-level jet (Pingel et al., 2016).

3. Methods

Remote sensing techniques were used for a preliminary mapping and for evaluating the general accessibility for the field campaign. More than 10 alluvial fans and fan remains were distinguished due to their location, height and erosional pattern. Aerial images and a DEM with a 30 m resolution were extracted from the USGS server to create maps for the field work. For further mapping after the field campaign, an extraction of the TanDEM was used, which provides a resultion of 12 m and is provided as a basemap within the final result plots.

Field mapping of Paleogene strata (Santa Bárbara Group) was carried out by Sophie Boven, while the height of the fans/fan ridges was additionally mapped with a dGPS-system (also included in the thesis of Sophie Boven). Parallel to that, samples were taken for OSL (optically stimulated luminescence)/IRSL (Infrared Stimulated Luminescence) and cosmogenic nuclide dating. Additional dating of Quaternary ash samples collected in the field will also be shown in the work of Sophie Boven.

In general, OSL dating was applied for most fans. Only along the highest and oldest alluvial fan OSL dating results might have given questionable results due to the saturation effects of this method. Hence, along the crest of the highest alluvial fan, a depth profile for cosmogenic nuclide dating was taken. Within the next chapters I will describe the methodology of each single method.

3.1. Field mapping and stratigraphic description

During the field mapping we recognized different geologic formations, Quaternary terraces and associated geologic structures. Fault planes, kinematic indicators and bedding planes were measured with a Krantz field compass and the FieldMove Clino App. Furthermore, a dGPS survey was conducted to estimate geometric and topographic characteristics of mapped alluvial fans. OSL- and the cosmogenic nuclide (depth profile) sampling were planned in advance according to the mapping results and lithologic distribution. At the sampling locations stratigraphic profiles were established and the best plumming locations (concerning OSL samples) were chosen based on the material of the single layers.

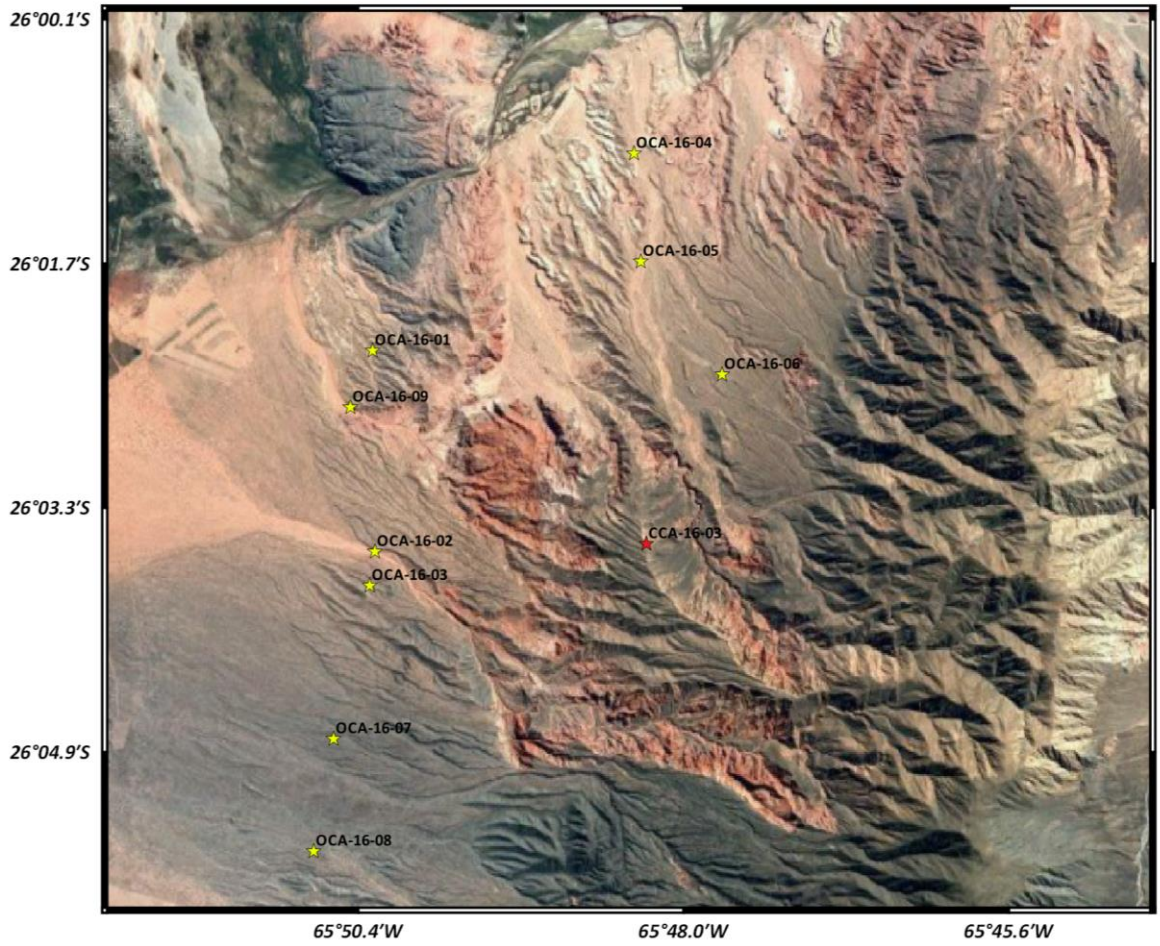

Figure 8 – The map is providing the locations of all OSL samples (yellow marker) as well as the cosmogenic nuclide sample (red marker).

(Basemap extracted from the Earth Explorer, 2017)

The distribution of the fans and the locations of all samples are shown in figure 8. Due to financial and time limitations not all samples could have been processed. Five OSL samples, namely 1,3,5,6 and 9 were dated and the results are being discussed in chapter 4.

The cosmogenic nuclide sample will also be discussed in chapter 4 since most of the necessary laboratory processing steps were carried out. Due to lack of time, the dating will be finished after the thesis submission.

3.2. OSL-Dating (Optically Stimulated Luminescence)

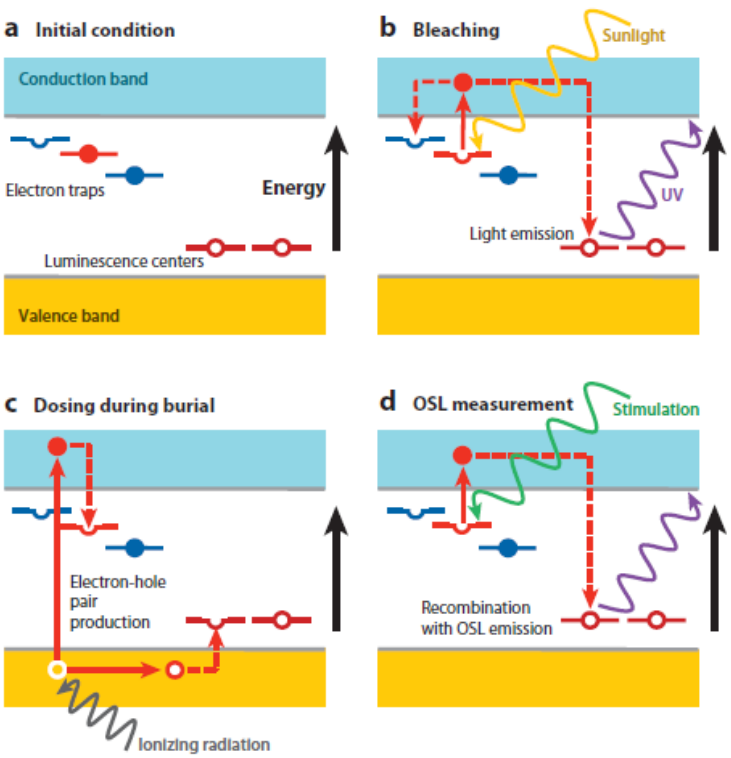

Figure 9 – Simplified band gap energy model of optically stimulated luminescence. Electron traps, which can be optically stimulated are shown in red, traps sensitive to thermoluminescence are marked blue.

(Rhodes, 2011)

3.2.1. Methodology

Optically Stimulated Luminescence is based on the observation that non electroconductive matter gets stimulated by light waves (specifically sunlight) and/or heat. A precondition to apply this technique is the occurrence of a lattice defect in the material of interest. Electrons are stimulated, which results in a shift to a higher energetic level. These electrons remain in such an energetic state if there is no further stimulation by light and/or heat; in case of renewed stimulation such as the radiation of light (luminescence), the electron returns to its initial state (see figure 9). Within the field of geology, the last exposure of sandy to silty sediments (K-feldspar and quartz crystals) to sunlight can be dated. This implies, that the exposure to light “zeroes” the current luminescence value of the sample (also called “bleaching”). When sediment gets covered by younger deposits, they are protected from further light radiation, and hence their luminescence value increases due to the occurrence of radioactive elements in the surrounding sediment. The age of the sample can then be recalculated in the lab due to the intensity of the emitted light, which is linked to the period the sample was shielded of sunlight by overlying sediments.

Taking this method into application, this automatically leads to the most important point, which is that samples cannot be exposed to any source of light during the field sampling and the subsequent laboratory preparation, except for red light with low intensity.

3.2.2. Field sampling

The sampling process was carried out based on the instruction by Nelson et al. (2015). Site selection was performed according to the accessibility and the occurrence of fine- to medium grained, low consolidated silty-sandy depositions. Three samples at different heights were taken at each site. Two of them were used for dating while a third one was kept in case of any lab or dating errors.

Sampling was conducted using non-transparent plastic tubes of a general length of 30 cm, wrapped with silver duct tape to avoid further exposure to light during excavation and sample transportation. After taking the samples by hammering the tube into an outcrop on the flank of an abounded alluvial fan, they were plugged with pieces of black foil stuffed into both ends of the tube and closed with duct tape again. The direction the tube was hammered into the fan is marked. During hammering it is important to prevent too much sediment mixing, due to the increase of luminescence intensity with depth towards the inner of the fan. This can be avoided by stuffing the remaining space within the tube. For further protection the tube was wrapped afterwards with additional dark foil and then boxed for shipping.

To gain information about the current material structure, water saturation as well as the amount of the existing radiating material within the sediments, a specimen of the sediments around the sample-hole was additionally taken (here no need for precautional measures).

3.2.3. Laboratory processing

Within the first step of the lab procedure, samples were carefully unwrapped from the side containing the closest sediments to the outcrop surface. After excluding the upper (probably sunlight exposed) few centimetres of datable material from the sampling tube, sediments were extracted, washed and sieved down to the fraction of 90-200µm. HCl (38%) was added with a little amount of H_2O_2 and left over night to dissolve carbonates and organic content. Samples were then washed and processed

by gravitational separation. In a first step, heavy minerals were separated using LST (Lithiumpolywolframate) heavy liquid with a density of 2.75 $\frac{g}{cm3}$. After washing and drying, quartz and feldspar bearing fractions were separated using LST with a density of 2.62 $\frac{g}{cm3}$. At this point, feldspar is ready for measuring, whereas the quartz is being further processed by another etching step with HF (38-40%) for 60min under permanent agitation and exposure to heat. Afterwards samples were washed, dried and sieved down to 90µm. The final output from this procedure was funnelled into small glass tubes for the luminescence measurement.

In an extra step conducted externally, the radiation of the sample-surrounding material (^{238}U, ^{232}Th and ^{40}K) was estimated with gamma spectrometry using high-purity Germanium well type detectors as well as a C Broad-Energy detector (both by Canberra Industries) at the GFZ Potsdam, which resulted in the given Dose rate D_o.

Table 1 *– SAR protocol for feldspar contaminated quartz, modified from Wallinga et. al (2002) for the OSL/quartz application and Buylaert et al. (2009) for IR-IRSL/feldspar.*

Step	OSL/Quartz	Post-IR-IRSL/Feldspar
1	Give dose[a], D_i	Give dose[a], D_i
2	Preheat, 240°C for 10s	Preheat, 270°C for 60s
3	Exposure to IR, 175°C for 100s	Exposure to IRSL, 50°C for 300s
4	Stimulate with blue, 40s at 110°C	Exposure to IRSL, 225°C for 300s
5	Give test dose, D_t	Give test dose, D_t
6	Heat to 220°C	Heat, 270°C for 60s
7	Expose to IR, 175°C for 100s	Exposure to IRSL, 50°C for 300s
8	Stimulate with blue, 40s at 110°C	Exposure to IRSL, 225°C for 300s
9	Repeat steps 1-8 for a range of D_i	Return to step 1

The luminecence measurements were carried out with two different approaches. The first one was common OSL dating by measuring the luminescence of quartz grains, using a SAR-protocol (single aliquot regenerative) for Feldspar-contaminated quartz by Wallinga et. al (2002; see table 1). An OSL reader by Lexsyg (Freiberg Instruments) was used, applying blue light for the OSL stimulation.

After first OSL stimulations of all samples it came clear, that most samples were too old for the OSL dating approach since results were exceeding 250Gy, which means, that the quartz grains were mostly saturated. Due to the high amounts of feldspar available, Infrared stimulated luminescence (IRSL) was chosen as an alternative dating method. This luminescence dating approach allows dating of older samples, but is also linked to a higher error than OSL dating (see chapter 5.1). The protocol of the IRSL dating was modified after the original approach by Buylaert et al. (2009; table 1).

3.3. Cosmogenic Nuclide Exposure – Dating (depth profile)

3.3.1. Methodology

Another approach to date the age of surfaces, which were previously exposed to sunlight is cosmogenic nuclide exposure dating. The theory behind this dating method is the assumption, that all exposed surfaces are permanently subjected to cosmogenic particles which are steadily irrupting the Earth's atmosphere. Their energy originates from supernova eruptions and causes the particles (nuclei, electrons, positrons) to accelerate due to the shock wave of the explosion while the particles themselves mostly derive from within the milky way (particles originating from the sun are being neglected due to their low impact on the Earth surface's material) (Dunai, 2010; Gosse & Phillips, 2001). Within the earth's atmosphere they create by interaction with atmospheric nuclei a secondary cosmic radiation (nucleons, protons, mesons) and are being energetically charged by the Earth's magnetic field. These secondary cosmic particles decrease with the approach of sealevel by bisecting approximately every 1500m (Dunai, 2010). The highest influx of cosmic particles is experienced the more vertical they approach the Earths' atmosphere meanwhile the lower the angle the higher the atmospheric depth they have to invade, leading to a decrease of particle influx.

Similar principles can be accounted for the impact on earths' surface with the difference of higher densities as well as changes in mean atomic mass and charge per nucleus (Dunai, 2010). The cosmogenic nuclides are then produced by the interaction of both types of cosmic-ray particles with atomic nuclei of

rocks/sediments, mostly during spallation (high energetic neutrons collide with atomic nuclei, resulting in a lighter nuclei as well as protons and neutrons). Starting from 1955, the discovery of several terrestrial in situ-produced cosmogenic radionuclides was reported. Within the field of Geosciences, ^{10}Be ($T_{1/2}$ = 1.36 ± 0.07 Ma) and ^{26}Al ($T_{1/2}$ = 0.708 ± 0.017 Ma; both values from Dunai, 2010) are the most common used ones due to their comparably long half-lives and their well-known production rates, which are barely influenced by environmental factors such as depth below surface, altitude etc. (Granger & Muzikar, 2001). They are both in situ produced within quartz grains. Just like in OSL dating, the timing of burial (shielding of further cosmic ray penetration by a sedimental cover) is dated based on the $^{26}Al/^{10}Be$ ratio and the assumption of exponential in situ production decrease towards zero beneath the surface.

3.3.2. Field sampling

Two different sampling methods are generally recommended for cosmogenic radionuclide dating: These include several samples from a depth profile by digging a 2 to 3 m deep and 1-m-large pit (Granger & Muzikar, 2001) or surface samples (hand-sized pieces) from the shielded side of >1m sized boulders, which should not have experienced any transport after sedimentation (Gosse & Phillips, 2001). The boulder sampling technique is rather easy to accomplish due to the comparably low amount of pre-scheduling. Owing the lack of high amounts of bigger boulders on the top of most fans, the depth profiling was chosen over the boulder sampling. Additionally, vertical sampling provides by the creation of a depth profile an estimation of inheritance due to previous exposure of the samples. For the location of the pit, the highest and most prominent fan within the study area was chosen. After the excavation of the hole, a stratigraphic profile was compiled and nine samples were taken at depths of (starting from the surface) 0 m, 0.3 m, 0.5 m, 0.65 m, 0.83 m, 1.0 m, 1.2 m, 1.4 m and 1.75 m.

3.3.3. Laboratory processing

The laboratory processing is based on a protocol established by the laboratory manager Bodo Bookhagen (Cosmogenic Isotopes Lab - Chemical Separation of Al and Be from Quartz-bearing rocks, published by Stanford University in 2007) and

was carried out at the Institute of Earth and Environmental Sciences of Potsdam University. In a first step samples were grinded and sieved down to a fraction of 250-500µm. Afterwards, a magnetic separation was performed before starting with the chemical treatment. To remove traces of Carbonate, organic material and other impurities samples were treated with 36% HCl in a 1:1 mixture with H_2O with a shot of H_2O_2 and heated on a stove over night under the fume hood. After washing and drying, the samples were further processed (similar to OSL sample preparation) by heavy liquid separation to remove further traces of heavy minerals as well as separate the feldspar from quartz also by applying LST concentrations of 2.75 $\frac{g}{cm3}$ and 2.62 $\frac{g}{cm3}$. The separation was completed through leeching in a 4l tank filled with a solution of 40% Hydrofluoric Acid and water (resulting in a 2% concentration for HF in this first step). After heating the sample in an ultrasonic bath over night (alternatively hotdog rollers) they were rinsed and washed. The leeching step was repeated with a HF concentration of 1% 2-3 times depending on the quality of the samples until a concentration of pure quartz was obtained.

After this final step, the samples will be sent for further analysis to external labsoratories. There, Berylium (and Aluminium) have to be chemically isolated in a first step from the other elements within the quartz grains and their concentrations have to be determined. Afterwards the Berylium and/or Aluminium fractions can be loaded into a target, to be analysed by AMS (Accelerated Mass Spectrometry). The research section of the Geological Department of the Institute of Earth and Environmental Sciences of Potsdam University commonly aims for the analysis of ^{10}Be due to its broader aging range compared to ^{26}Al.

4. Results

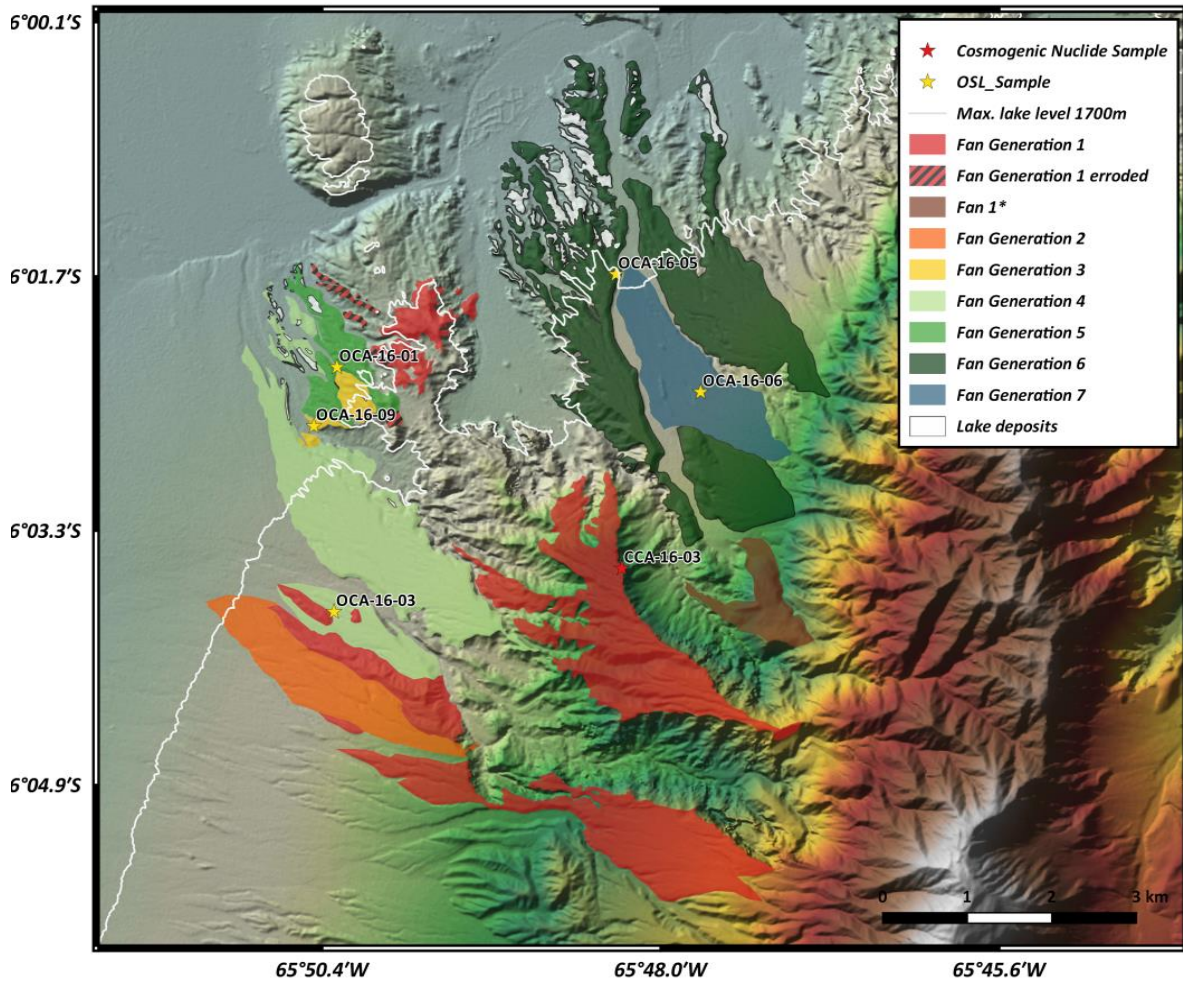

Figure 10 – Overview map of all fan generations within the study area as well as the locations of all further processed samples. The white line indicates the maximum lake level at 1700 m linked to the lake that existed between ~13.5 ka and 4.8 ka. The fans were mapped on a DEM extract of the tanDEM-project with a 12 m resolution and a hillshade layer on top.

Within this chapter I will present the outcomes of this study. Figure 10 shows the distribution of the 7(/8) fan generations mapped based on remote sensing, field observations and the dating results. The distribution and connection of the single generations will be further discussed in chapter 5. The results of the OSL/IRSL dating as well as site characteristics will be described in the following.

4.1. Sampling site characteristics

4.1.1. OSL-Sampling Site 1 (OCA-16-01)

Collected: 10.05.2016, 10:00 am.

Location: S -26°02'15.5" / W -65°50'17.7"

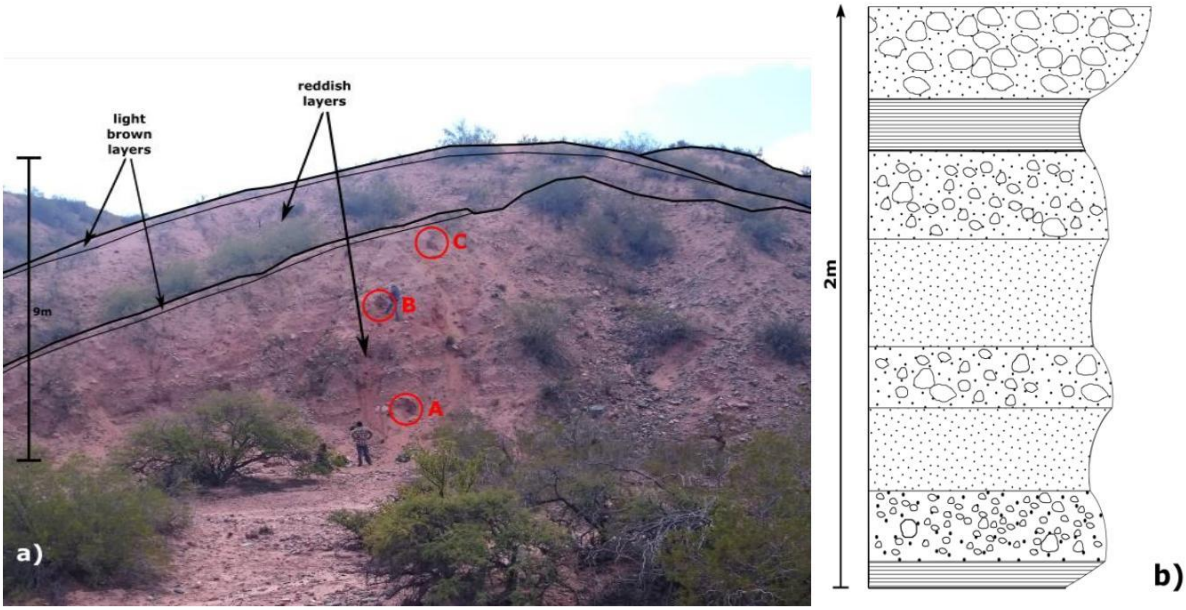

Figure 11 – Overview of the sampling site 1 (a) and the generalized stratigraphy (b). In (a) the difference of the main reddish fan-strata is visible next to a light brown layer that is deposited on top of it. Sampling spots A, B and C are marked by the red circles (viewing angle NNE). In b) an example of the stratigraphy is being provided (taken at the base around hole A) with very fine-grained sand at the base passing upwards to coarse-grained matrix supported conglomerates and pebbly sandstones.

Site 1 is characterized by an alternation of subhorizontally (bedding estimation: 312/14) deposited reddish and brown strata (see fig. 11a). The light brown layers were on top of the fan deposits and showed a medium- to coarse-grained (partly up to fine silt) matrix of sandstones with subangular quartz pebbes (diameter 0.5-2 cm; figure 11b). The red layers are matrix supported conglomerates, where the matrix consists of medium-grained sand up to silt, while pebbles made by subrounded clasts (diameter of 1-10 cm) of metamorphics and more rounded pebbles (diameter of 1-3 cm) of metamorphic (70%) and granitic rocks (30%). Within the finer sections no layering was visible.

Samples were collected at 5 and 8 m (B and C, respectively), relatively to the lowermost sampleing point (A equal to 0 m; see figure 11a).

4.1.2. OSL Sampling Site 3 (OCA-16-03)

Collected: 10.05.2016, 05:00 pm.

Location: S -26°03'49" / W -65°50'19"

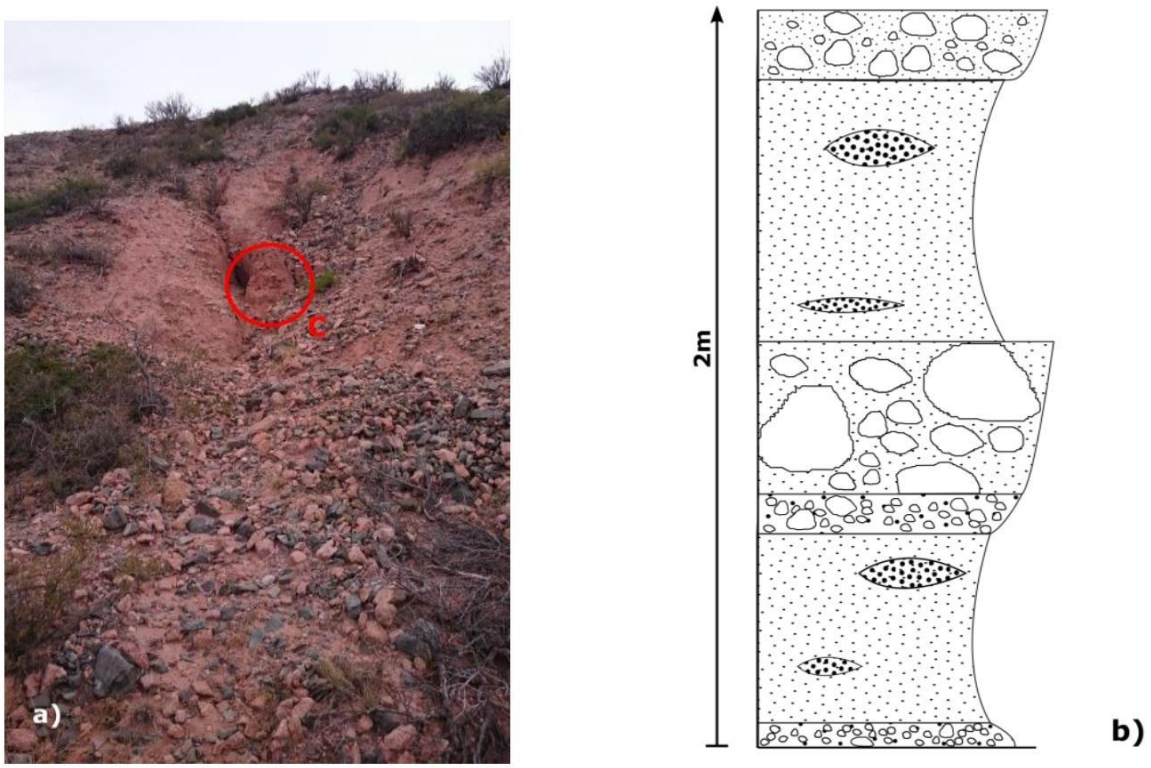

Figure 12 – Overview of the sampling site 3 (a) and the generalized stratigraphy (b). a) provides a look from a lower angle to the dating spot 03-C (viewing angle NNE).

The OSL sampling site 3 is dominated by fine grained reddish-beige sand layers with average thicknesses of 1-2 m, a subhorizontal bedding and contain only few pebbles. Within those sandy deposits, lenses of medium- to coarse-grained sandstones are occurring (figure 12b). The sand layers are interrupted by ~0.5-m-thick poorly-sorted, matrix-supported conglomeratic layers. Clasts are subangular to subrounded in shape with a diameter of up to 0.5 m and a source composition of 60% metamorphic and 40% granitic rocks. The outcrop was estimated to be 13 m high with the sample hole locations 6 and 10 m (B and C, respectively), relative to lowermost sampling hole A (figure 12a).

4.1.3. OSL Sampling Site 5 (OCA-16-05)

Collected: 11.05.2016, 11:30 am.

Location: S -26°01'40" / W -65°48'19"

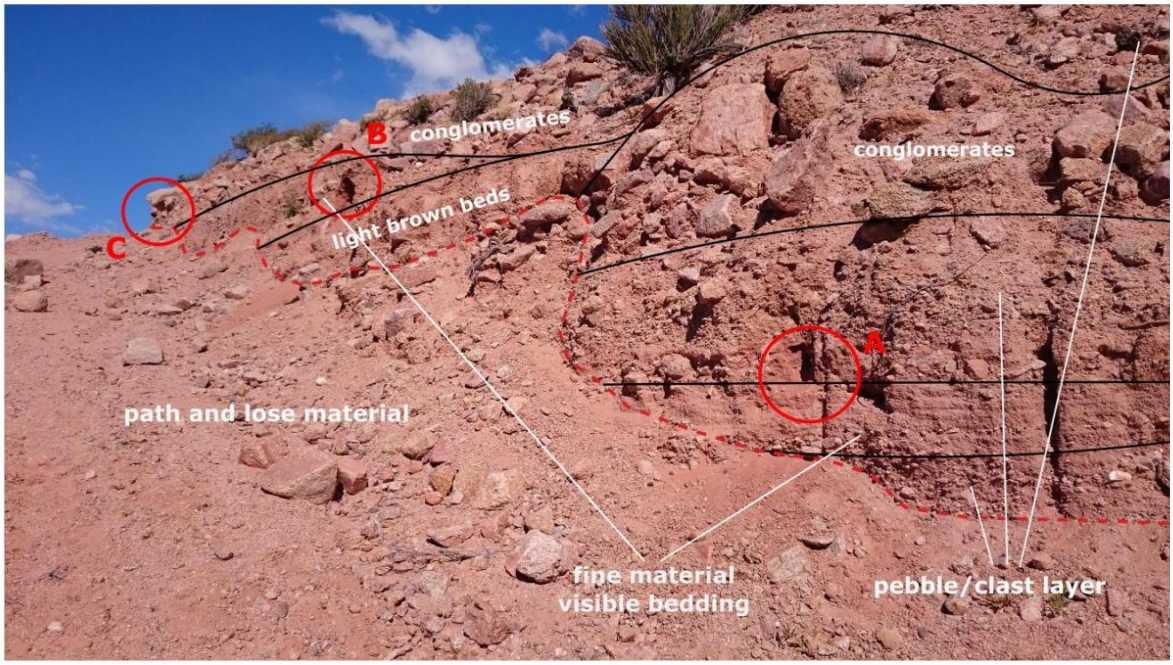

Figure 13 – Overview of sampling site 5. Different types of strata (conglomerates, pebble/clast layer…) are marked in the picture; sampling holes A, B and C are emphasized by red circles (viewing angle WNW).

Site 5 was located along a ca. 30-m-high incised aluvial fan with an estimated bedding of 102/12 (figure 13). Samples were collected in the upper section at an estimated height of 15 m (on top of some lower cliffs), because the lowermost beds were too cemented to allow penetration of the sampling tubes. The sample holes are spread over a distance of 10 m parallel to the hiking path and have an estimated height difference of 1 m from one hole to the next (for example from A to B). Here bedding was estimated to be 102/12 (dip direction-dip angle).

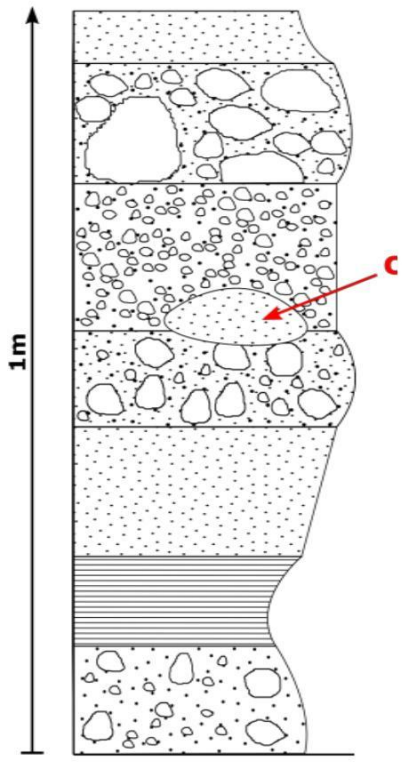

Figure 14 – Generalized stratigraphy at sampling hole 05-C.

The sampled section consists of grey to reddish matrix supported conglomerates alternated with finer beds exhibiting a crude bedding. The general

clast material source was granite and therefor rich in quarz. The finer reddish beds show an average thickness of 20 cm and consist of coarse- to medium-grained sandstones. The light brown beds mainly included coarse sand with small quarz pebbles; an average thickness of 20 cm was observable. Finally, the outcrop includes a conglomeratic layer very rich in subrounded pebbles (1-2 cm), clasts (3-10 cm) and boulders (10-50 cm) of granitic origin (figure 14).

4.1.4. OSL Sampling Site 6 (OCA-16-06)

Collected: 11.05.2016, 03:00 pm.
Location: S -26°02'25" / W -65°47'43"

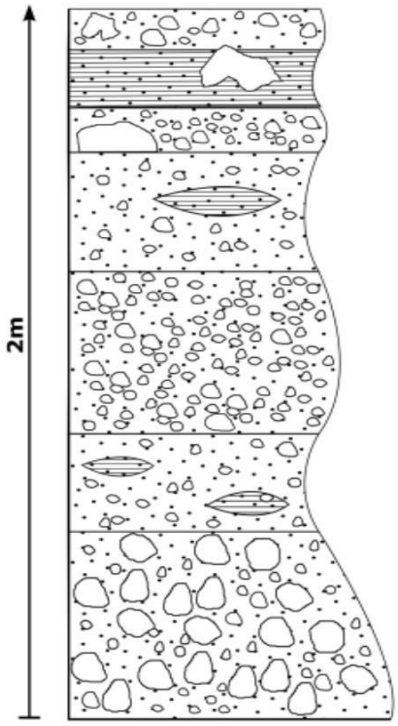

Figure 15 – Generalized stratigraphy for sampling site 06-B.

Site 6 was located along a modern river channel with an estimated bedding of 306/12 (almost parallel to the channel ground, see figure 16). Sample A and C are both located at the left side of the channel whereas B is on the right. A and B are 10 m apart, B and C another 8 m. The height difference of the single samples is estimated to be 1 m, starting with hole A 0.5 m above ground.

Sampled deposits include matrix-supported (coarse sand, partly silty) conglomerates very rich in clasts, which are 3 to 20 cm in size, mostly subangular of granitic origin and lenses of pebbly siltstones to sandstones. Locally, bigger blocks up to 1.5 m in size, can be found (see figure 15). It should be finally notes, that these conglomerates are rich in angular quarz pebbles ranging in size from 1 to 3 cm.

Figure 16 – Overview of the OSL sampling site 6. The site was located along an active river channel; samples were taken at different elevations along the riverbanks (viewing angle ESE).

4.1.5. OSL Sampling Site 9 (OCA-16-09)

Collected: 18.05.2016, 10:30 am.

Location: S -26°02'37.8" / W -65°50'27.4"

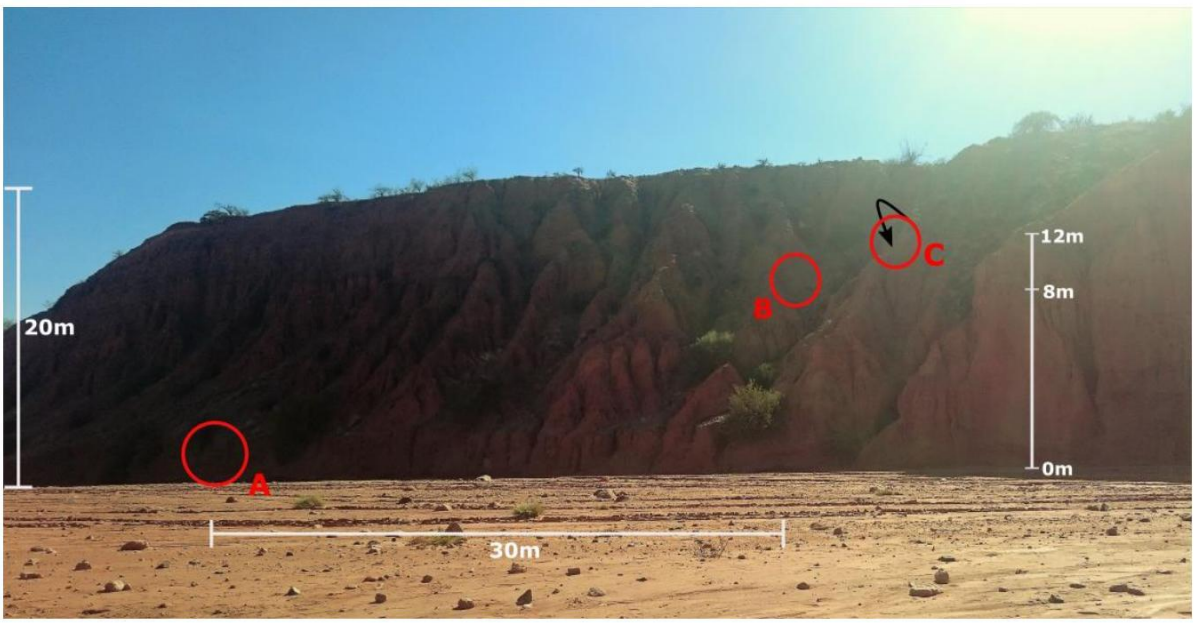

Figure 17 – Overview of the sampling site 9, the highest sampled outcrop location (viewing angle NNE).

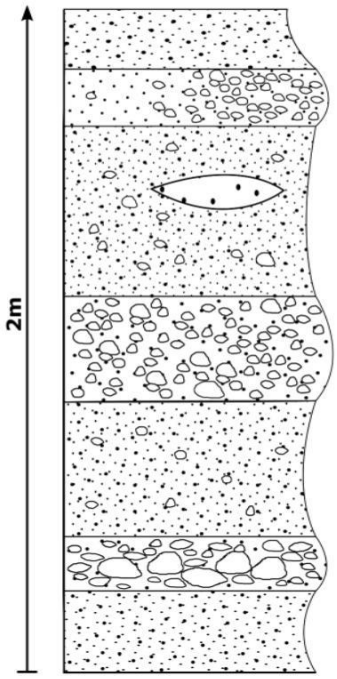

Figure 18 – Generalized stratigraphic column of site 9.

Site 9 provided the highest outcrop location for OSL dating (around 20 m) with an estimated bedding angle of 20° (see figure 17). Samples were taken at relative heights of A, 0 m, B, 8 m and C, 12 m. These deposits include 10- to 70-cm-thick, matrix-supported, conglomerates exhibiting a crude bedding with a red-coloured matrix, consisting of fine to coarse grained sand rich in quartz. Clasts are subrounded, have a diameter of 5 to 10 cm and are composed of metamorphics (70%) and granites (30%). These deposits are alternated with up to 2-m-thick pebbly sandstones. Within these beds we can also find coarse grained sand lenses which are partly very cemented (generalized stratigraphic column in figure 18).

4.1.6. Cosmogenic nuclide sampling (sampling site 7, CCA-16-03)

Collected: 12.05.2016, 02:00 pm.
Location: S -26°03'32.4" / W -65°48'16.5"

The most elevated and therefore oldest alluvial fan in the area was sampled for cosmogenic nuclide dating. As mentioned in the Methods section, this morphology was selected because OSL is not suitable for deposits older than Upper Pleistocene. An overview of the sampling location of this alluvial fan is shown in figure 20. The bedding for this site was estimated 014/06 (dip direction/dip angle). Nine samples were collected from a depth profile are located at depths of (starting from the surface) 0m, 0.3m, 0.5m, 0.65m, 0.83m, 1.0m, 1.2m, 1.4m and 1.75m. The stratigraphy observed in the hole is shown in figure 19. A table for the measured shielding values at the site can be found in the Appendix, table 2.

The laboratory work is still in progress so results will be ready after the conclusion of this thesis.

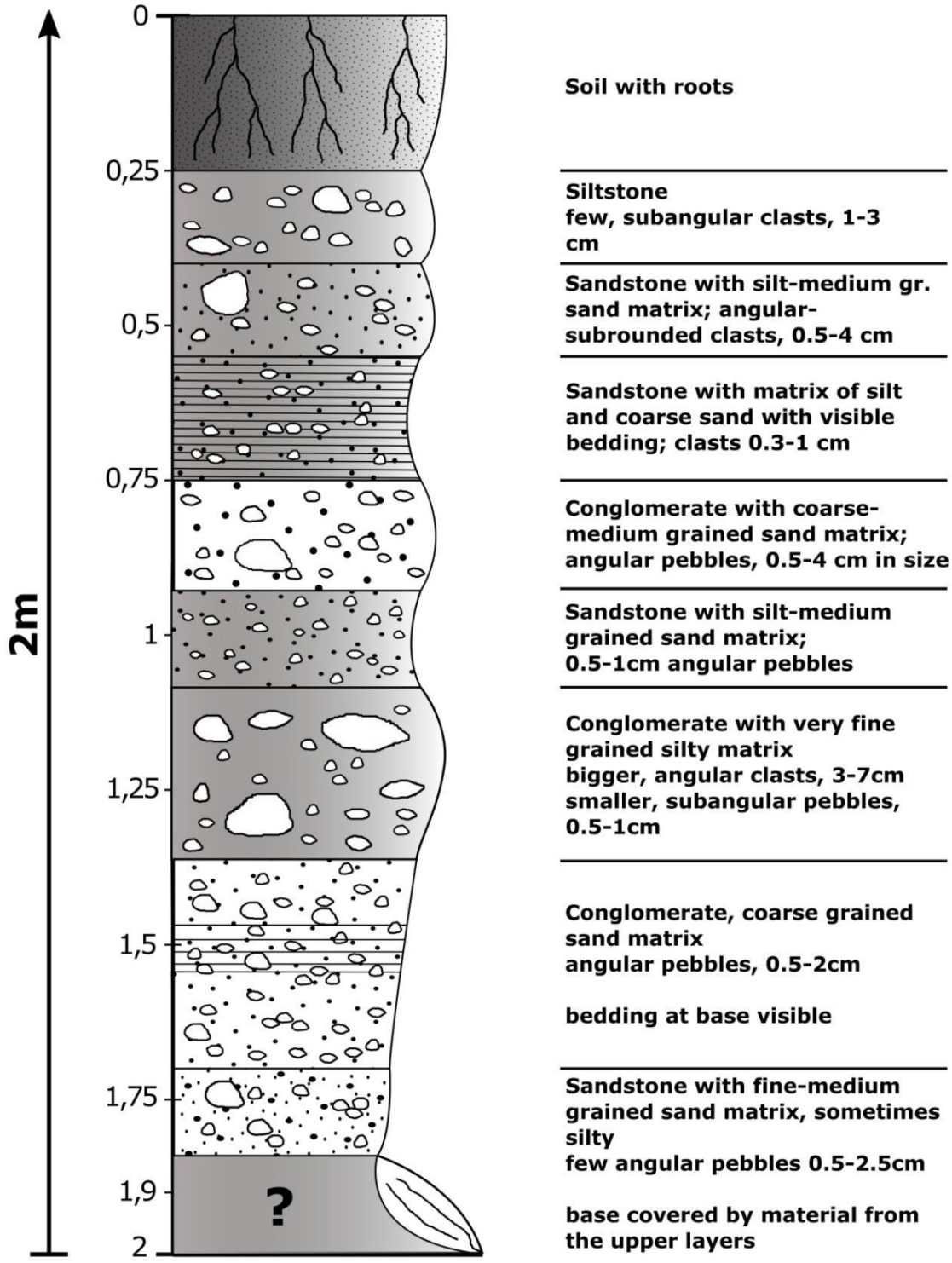

Figure 19 – Stratigraphy of the depth profile sampled for cosmogenic nuclide dating.

Figure 20 – Overview of the alluvial fan chosen for cosmogenic nuclide sampling, which is also the main fan dominating the study site due to its wide distribution. The red circle marks the sampling location for the depth profile (viewing angle ESE).

4.2. Geochronology results

Within this study two different dating methods were applied. The results of the 12 OSL / IRSL samples are discussed in the following chapter. The results from cosmogenic nuclide dating are not yet available, therefore will be reported in the thesis of Sophie Boven which is still in progress.

4.2.1. OSL-results

OSL results were processed with the Dose Rate and Age Calculator (DRAC) of Aberystwyth University (version 1.2, www.aber.ac.uk/en/dges/research/quaternary/luminescence-research-laboratory/dose-rate-calculator/, available for OSL and thermoluminescence dating). For the age estimation several inputs are needed such as basic information about the sampling location (GPS-Coordinates, altitude, material coverage etc.) and the amount of radiation from surrounding sediments (mostly produced by the decay of ^{238}U, ^{232}Th and ^{40}K), which was obtained by gamma spectrometrical measurements.

Within the first measurements with the classic OSL approach on quartz grains, the younger alluvial fan generations were properly dated within a reasonable standard

deviation. Instead, the error for older fans was too large since the saturation of quartz is reached at a mean value of 250 Gray and most samples were exceeding this value. So a second dating approach was carried out by using feldspar grains. The saturation of feldspar is higher than quartz, but it also includes higher errors. To get the best results, a SAR-("single aliquot regenerative") protocol for feldspar (also post-IR-IRSL protocol by Buylaert et al., 2009) was refined from the original SAR-protocol used for quartz measurements (Murray & Wintle, 2000; Murray & Wintle, 2003; Wintle & Murray 2006). A higher measurement temperature of 225°C was used, to reach the deep electron traps, which suffer less of bleaching effects. For two sampling locations a third sample was processed due to large (estimated) errors of the first two samples at each site. A full compilation of results is shown in table 3. The first sampling location OCA-16-01 (fan generation 5), provided two ages of 147.3 ± 14.9 ka (hole A at 1628m of elevation) and 168.4 ± 13.5 ka for sampling hole B (1633m of elevation). The lower age of the relatively lower located sample A might be caused due to the erosion and redeposition of previous higher (and thus younger) deposits. Since overlapping occurs within the range of errors, the mean age of the site is still considered to be consistent.

Sample OCA-16-03 provided an age of 223.8 ± 15.3 ka (hole A, 1737 m), while sample B (6m above A) yielded 215.9 ± 20.5 ka. Although these ages overlap within the error bars, they would indicate due to a time difference of 7.9 ka a sedimentationrate of ca. 0.759 $\frac{mm}{yr}$ for fan 4.

Sampling location OCA-16-05 shows comparably young fan ages with 86.8 ± 8.1 ka at hole A (altitude – 1673 m) and 82.2 ± 7.9 ka at point C (1676 m). Although these ages overlap within the error bars, they would indicate a sedimentation rate of ca. 0.652 $\frac{mm}{yr}$ for fan generation 6, which is compatible with the one estimated for the Alluvial Fan 4

Sampling site OCA-16-06 (fan 7) yielded two ages of 0.4 ± 0.1 ka for hole A and 13.1 ± 2.3 ka for hole C (1792 and 1794 m of elevation, respectively). Sample B was processed in a second step and provided an age of 2.1 ± 0.5 ka (1793 m of elevation).

The last sampling site OCA-16-09 (alluvial fan generation 3) yielded the oldest ages. All three samples were dated because sample A (altitude of 1630 m) gave a result of 6.2 ± 1.0 ka, while sample B (1638 m) and C (1642 m) yielded 271.8 ± 24.5 ka and 245.3 ± 19.0 ka. Due to these results, A was considered to originate from a comparably recent deposition of the new fan crosscutting the old fan depositions. In this case, although the ages overlay within the error bars, a sedimentation rate of 0.151 $\frac{mm}{yr}$ between sampling site B and C can be estimated.

Sample	Altitude	Depth	No. of aliquots (selected / total),	Uranium (U-238)	Thorium (Th-232)	Potassium	Cosmic dose rate	Water cont. measured	Dose rate (D_0)	Equivalent dose (D_e) [Gy]	Equivalent dose distribution characteristics			OSL age [ka]
	[m NN]	[m]		[ppm]	[ppm]	[%]	[Gy/ka]	[%]	[Gy/ka]	CAM	Standard deviation [%]	Over-dispersion [%]	Skewness	CAM
OCA-16-01A	1628	9 ± 1	6/6	1.9 ± 0.1	13.0 ± 0.17	2.22 ± 0.11	0.08 ± 0.01	1,0	4.38 ± 0.27	644.6 ± 51.3	21.6	18.4	0.63	**147.3 ± 14.9**
OCA-16-01B	1633	4 ± 0.5	6/6	2.31 ± 0.19	14.01 ± 0.52	2.31 ± 0.12	0.15 ± 0.02	1,8	4.74 ± 0.29	797.4 ± 41.6	14.1	10.0	0.19	**168.4 ± 13.5**
OCA-16-03A	1737	10 ± 1	6/6	2.89 ± 0.06	13.94 ± 0.32	2.03 ± 0.1	0.08 ± 0.01	4,1	4.57 ± 0.29	1022.9 ± 27.8	6.7	0	0	**223.8 ± 15.3**
OCA-16-03B	1743	4 ± 0.5	6/6	2.75 ± 0.26	12.41 ± 0.86	2.07 ± 0.1	0.15 ± 0.02	0,7	4.5 ± 0.28	972.6 ± 68.9	18.8	12.9	-0.03	**215.9 ± 20.5**
OCA-16-05A	1673	5 ± 0.5	6/6	3.84 ± 0.23	23.5 ± 0.52	3.68 ± 0.18	0.13 ± 0.01	0,2	7.3 ± 0.4	633.4 ± 47.9	19.1	17.3	-0.35	**86.8 ± 8.1**
OCA-16-05C	1676	2 ± 0.5	6/6	3.25 ± 0.24	16.65 ± 0.32	2.38 ± 0.12	0.19 ± 0.02	1,3	5.36 ± 0.32	440.4 ± 33.6	21.5	17.9	0.91	**82.2 ± 7.9**
OCA-16-06A	1792	3 ± 0.5	5/6	10.7 ± 0.33	44.83 ± 0.81	3.7 ± 0.19	0.17 ± 0.02	1,3	11.28 ± 0.69	4.3 ± 0.5	28.9	25.1	0.33	**0.4 ± 0.1**
OCA-16-06B	1793	2 ± 0.5	5/6	8.88 ± 0.11	41.06 ± 1.67	3.9 ± 0.2	0.2 ± 0.02	0,3	10.62 ± 0.63	22.1 ± 5.2	69.8	51.8	1.91	**2.1 ± 0.5**
OCA-16-06C	1794	1 ± 0.5	6/6	11.73 ± 0.58	52.36 ± 2.86	3.76 ± 0.19	0.22 ± 0.02	0,4	12.36 ± 0.79	161.5 ± 26.6	39.8	40.2	-0.08	**13.1 ± 2.3**
OCA-16-09A	1630	20 ± 1	6/6	1.62 ± 0.03	8.42 ± 0.3	2.22 ± 0.11	0.03 ± 0.003	0,1	3.84 ± 0.25	23.7 ± 3.4	36.6	35.5	0.06	**6.2 ± 1.0**
OCA-16-09B	1638	12 ± 1	6/6	1.33 ± 0.08	6.53 ± 0.59	1.74 ± 0.09	0.06 ± 0.01	0,2	3.17 ± 0.23	861.0 ± 46.3	15.4	9.1	0.68	**271.8 ± 24.5**
OCA-16-09C	1642	8 ± 1	6/6	1.07 ± 0.06	5.64 ± 0.44	1.99 ± 0.1	0.09 ± 0.01	0,2	3.28 ± 0.23	803.7 ± 27.1	10.9	0	1.01	**245.3 ± 19.0**

***Table 3** – Results of the IRSL measurements with feldspar at 225°C.*

5. Discussion

5.1. Dating reliability

One major problem during the sample preparation for dating occurred while etching the samples. In most cases it was rather impossible to get rid of the feldspar remains and obtain pure quartz, because etching can only be carried out for a limited amount of reruns (not only due to the costs of HF but mainly because the quartz grains would be too corroded and in case of OSL, too small for dating). Therefore, for the OSL technique, measurement errors were encountered because a signal from remains of Feldspar (IR signal) was superimposed to the main quartz-signal.

Another issue during OSL dating occurred because quartz reaches a saturation level at 250 Gy. Measurements showing results higher than 250 Gy are generally saturated and hence they underestimate real ages. This particular problem occurred for most samples (notably OCA-16-01B, OCA-16-03A+B, OCA-16-05A+C and OCA-16-09B+C). An alternative approach to the use of quartz is dating of feldspar minerals. They have a higher saturation level than quartz minerals, but show a general underestimation of ages, since natural fading ("anomalous fading") in darkness without further artificial stimulation occurs. Compared to quartz, feldspar needs much more time of exposure until all electrons return to their initial state. In return, this may lead to an overestimation of the ages and compensate (or probably overcompensate) the anomalous fading.

To avoid the problem of the anomalous fading a post-IR-IRSL protocol was used, which was accomplished with a preheating step at a level of 50°C before the final measurement at a level of 225°C. With this procedure the deep electron traps can be reached, while samples are generally not getting affected by the natural fading. Since anomalous fading isn't an issue with deep electron traps, artificial bleaching during the measurements might sometimes not be fully effective. In conclusion, similar ages for quartz and feldspar of younger samples let me assuming that full bleaching of the deep traps using the post-IR-IRSL protocol is successful for all the samples.

Another problem might be the OSL sample placement at location 5 and 6. Sample location 5 provides good ages that fit within an error with a mean age of 84.5 ± 8 ka.

Due to the choice of the sampling location on top of some more cemented cliffs, these ages might not represent the maximum age of the fan.

For sample 6 the riverbanks of a modern river incising fan 7 was chosen due to its comparably young age. The deposits of this fan are not very thick or eroded and thus lack access to major outcrops (compared to other fan generations within the study area). The results most probably reflect different generations of recent river deposits along the modern river. The oldest age of 13.1 ± 2.3 ka is most likely an underestimation of the actual fan age. Nevertheless, due to its low elevation, alluvial fan 7 represents the youngest deposit of all studied fans within the study area.

5.2. Fan generations and depositional succession

Within our study area we observed and mapped 7 generations of alluvial fans (figure 10, chapter 4). The highest alluvial fan generation has not been dated yet (cosmogenic nuclide dating in progress); however, its age is thought to be 1.5-2 Ma like the oldest pediment surface to the south of the study area, dated by Strecker et al. (1989). This age was assumed for the main fan at the center of the study area (location for the cosmogenic nuclide dating) and is also applied for another alluvial fan at a similar elevation to the south (Fig. 10). Further remains of the alluvial fan generation 1 were mapped in the south-southeast of the Loma Negra basement block and north of alluvial fan generation 2, as documented by topographic profiles and other characteristics, like the color of outcrops, composition of clasts and erosional patterns (Fig.10 for overview; profiles 1, 3, 4 and 10 in Fig. 23 and 24 in the Appendix). Along the south-western flank of the Loma Negra several highly eroded remains of fan generation 1 were also observed (Fig. 10, dashed line pattern). These remnants were probably uplifted during the deformation of the basement block. Fan 1* (Fig. 10; profile 3 in Fig. 23 and 24, Appendix) is the head of a fan, which is due to topographic profile comparison expected to represent an intermediate generation of fan generations 1 and 6. Due to extensive erosion of most parts of this alluvial fan, it is hard to understand, if it was previously connected to alluvial fan generation 6 and later on uplifted and eroded, or if it represents another fan generation within fan generation 1 and 6 due to its higher elevation compared to generation 6. Further dating might be helpful to resolve this question.

Alluvial fan 2 incised the alluvial fan generation 1 in the south-western part of the study area and shows a darker color with a clast composition of 70-90% Schist and 10-30% Granite. The sediment sources area is mainly from the Puncoviscana section exposed in the center of the Filo Paranilla (Fig. 22, Apendix).

Alluvial fan generation 3 provides the oldest age results (271.8 ± 24.5 ka and 245.3 ± 19 ka). The fan remains were mapped based on the height- and color-differences to the adjacent fans (Fig. 10). The lack of preserved alluvial fan heads suggest erosion and redeposition of material originating from the central sectors of alluvial fan 1, which in turn is connected to the drainage system of the Filo Paranilla. The same may have occurred in relation to deposition of alluvial fan generation 5, where ages of 147.3 ± 14.9 and 168.4 ± 13.5 ka were obtained. It is assumed, that this fan incised alluvial fan 3 and was deposited clasping around the remaining depositions of fan 3. For sampling site 1 we also observed an inversion of expected ages, getting a lower age from a respectively lower sampling hole. A reason might be the erodion and redeposition of younger material at the base of the fan. Due to this error, the assumption of a medium age value of 157.85 ± 14.2 ka might be reasonable for this dating site.

The alluvial fan generation 4 is relatively well preserved and is located between the remains of fan 1 and the alluvial fans 3 and 5. Despite the cutting of the head of the fan and the incision of the most current fan within the area (not part of this study) into fan 4, the distribution can be well observed based on the lower amount of erosion of the fan surface as well as a light coloring and the height profile comparison to fan 1, 3 and 5 (overview Fig. 10; profiles 1 and 5, Fig. 23 and 24, Appendix). Site 3 provided ages of 215.9 ± 20.5 and 223.8 ±15.3 ka, which overlap perfectly within the error bar. At the northwestern terminations of the fan, remains of lake deposits are onlapping the alluvium.

Alluvial fan generation 6 provides the most preserved set of fans, even though we also partly observe erosion between the head and the downhill section of the fan (southernmost section of the fan, Fig. 10). In the north, lake deposits are onlapping on the fan sediments. As discussed in the previous section, the obtained ages at site 5 are reliable concerning the processing, but might not provide the full age range of

the fan. Nevertheless, 82.2 ± 7.9 – 86.8 ± 8.1 ka provide good results and are assumed to represent the age of fan generation 6.

Alluvial fan generation 7 was incised and accumulated after the deposition of the fan generation 6 (Fig. 10 for overview; profile 9 in Fig. 23 and 24 in the Appendix). As discussed in the previous section, the oldest age obtained for this site of 13.1 ± 2.3 ka might not reflect the depositional age of the fan but rather date a deposition of the modern river incising the fan.

A major influence on the erosive appearance of most fans within the area and the disconnection of the alluvial deposits superimposed on the Loma Negra basement block of the source/headers, was the occurrence of the paleolake (described in chapter 2.2), which we assume to have eroded, removed and redistributed lots of the Quaternary and Tertiary deposits within the study area (see figure 10; 1700m contour corresponding to the lake level maximum ~14 ka; Hermanns et al., 2004). Due to the lack of connectivity, further sampling within the area should be accomplished, specifically for the fan depositions next to the Loma Negra basement block.

5.3. Tectonic influences on fan deposition

As observed by Strecker et al. (1989) for the region south of the study area, the Santa Maria Valley provides abundant evidences for ongoing tectonic activity until at least ~0.6 Ma. Grier et al. (1991) and Carrera et al. (2006) also report ongoing reactivation of Cretaceous extensional during Andean contraction. This assumption is supported by additional observations, like for example those of Hilley & Strecker (2005), who reported onset of conglomeratic terrace aggradation sometime during the last 0.98 Ma within the Toro basin (few tens of km to the north to the study area) behind an uplifted bedrock block. Within the study area the occurrence of tectonic activities is also thought to have played a role in the occurrence of rock avalanches in the Quaternary, although more humid conditions have been invoked (Trauth & Strecker, 1999; Hermanns et al., 2006). Based on this knowledge it can be assumed, that the alluvial fans within the area might partly be tectonically imprinted. An effect of post-deposition uplift partly occurs at the southwestern edge of fan 7, where two small rises trending NNW-SSE and another bigger hill a few meters to the south at the edge of the southernmost fan of generation 6 are located (Fig. 10; profile 2 in Fig. 24 shows the uplifted section in fan generation 6). These features mostly consisted of

uplifted granite blocks accompanied by incompetent sediments of the Maiz Gordo Formation. The location of modern river incision probably cross cutting fan 6 directly on the eastern side of the granites might be attributed to a zone of material weakening associated with the granite uplift. Another evidence is based on the intense erosion of older fans (generation 1,2,3 and 5), especially the central sector of fan 1 and the depositions next to the Loma Negra. In between disconnected deposits around the Loma Negra and the central fan 1, deformed units of the Santa Bárbara Subgroup are visible. This section is both influenced by the moderate reactivation of former extensional structures in a contractional manner and probably part of the anticlinal axis along the Loma Negra basement uplift (based on geological maps of Grier et al., 1991 and Carrera et al., 2006). Uplift and/or deformation of a highly eroded alluvial fan can also be observed in the south of the study area (Fig. 10). Further input might be given by the results of Sophie Boven. Nevertheless, a tectonic influence based on renewed uplift of the Filo Paranilla and associated structures might partly influence the occurrence of fan generations. The link of tectonic activity to fan occurrence within the area would however need further dating support. Regarding the short time frame this study incorporates, tectonic activities might most likely have had only side effects on fan accumulation in the study area within the Quaternary.

5.4. Climatic influences on fan deposition

Apart from tectonic factors, climatic variability can also be a major controlling force because it affects sediment supply and water discharge, which in turn influence erosion, incision and accumulation processes (although rock erodibility might be, as previously discussed, related to tectonic activity). Specifically, runoff is connected to the regional climate, which is highly influenced by tectonic uplift and shielding effects (see chapter 2). Within the study area, erosional denudation is mostly influenced by periodic precipitation from moist air masses deriving from the South American Low Level Jet that crosses the orographic barrier of the Cumbres Calchaquíes as indicated by Bookhagen & Strecker (2012). In Figure 21 an extraction of the global benthic oxygen isotope record (Lisiecki & Raymo, 2009) is plotted against $CaCO_3$ concentrations and saline diatom quantities from a drill core at lake Titicaca (Altiplano-Puna Plateau; Fritz et al., 2007), the closest paleoclimatic record to the

study area. Below the results of the OSL dating are shown in combination with the respective fan generations plotted in relative height differences. Grey bars indicate dry and warm periods in the Plateau region, which correlate with global interglacial stages. In particular, in the Central Andes, increased precipitation and/or reduced evaporation was reported by several studies during these glacial periods (Haselton et a., 2002; Fritz et al., 2007; Baker & Fritz, 2015). Similar observations were made by Baker &Fritz (2015) specifically for the Sierras Pampeanas. Comparing the results of my study with the climatic records, alluvial fan accumulation phases correlate with global glacial periods and wet phases in the Central Andes. The gaps in between the

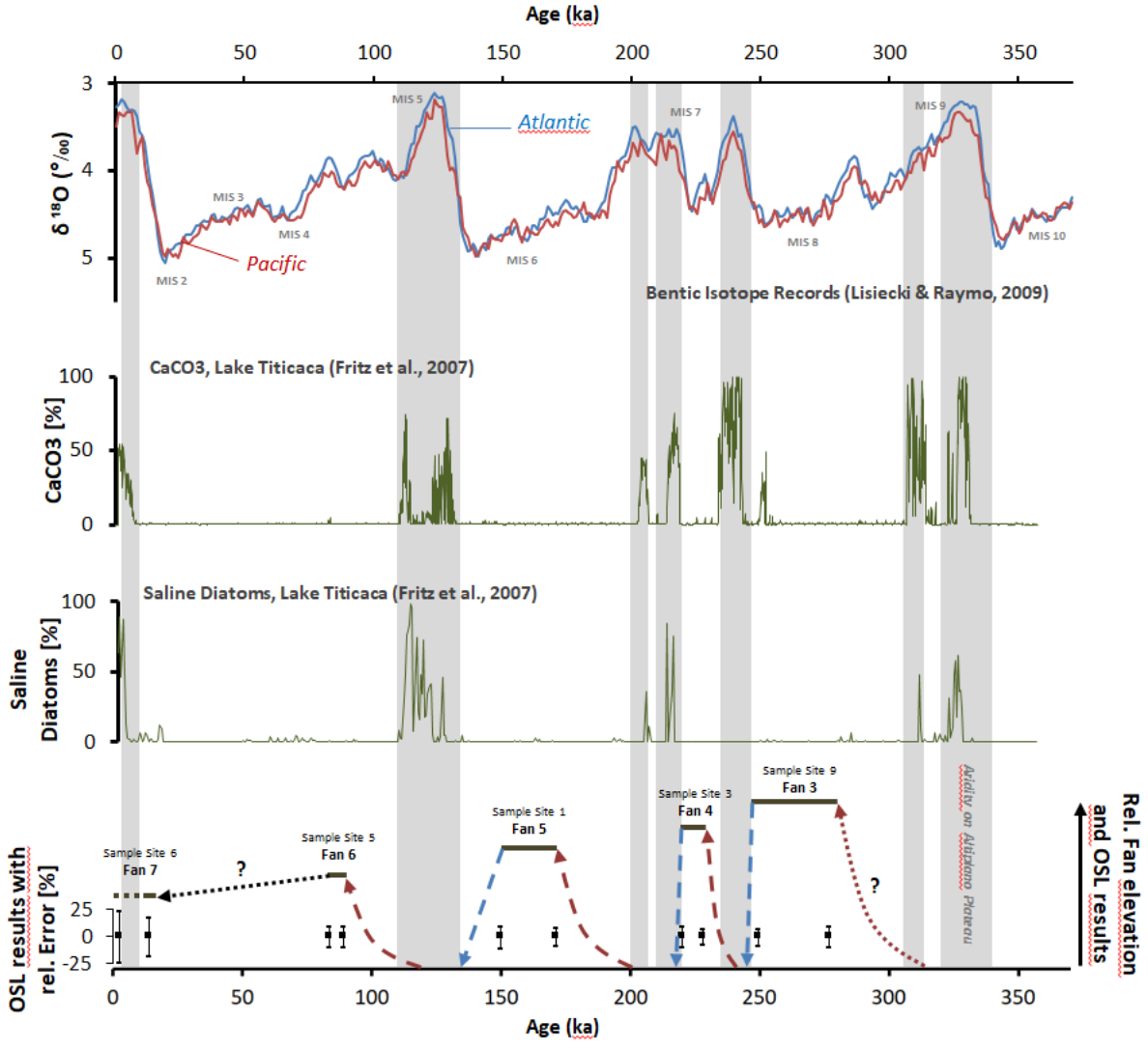

Figure 21 – Comparison of climatic proxies from the region with the results of OSL dating. Grey bars show arid phases linked to lake proxies (Fritz et al.,2007), which also match with benthic isotope records (Lisiecki & Raymo, 2009) from the Pacific (red) and the Atlantic (blue). Note that the OSL values (alluvial fan deposits) correlate with transitional phases to glacial maxima for the timing of fan deposition.

data are consequently assumed to illustrate phases of incision, which correlate with interglacial (and possibly part of glacial) periods (MIS maxima) corresponding to warm, dry conditions on the Altiplano. Based on these findings, I assume an increase in sediments and debris availability in the source region during the warm and dry phases (global interglacials), which may be facilitated by the decrease in vegetation. This material will be transported and redeposited downslope by rivers (alluvial fan development) during the following glacial phase, when increased precipitation will trigger higher water saturation in debris and sediments. The system will then tend to a state of equilibrium concerning the Q_s/Q_w-ratio (supply of sediments/water), until the vegetation cover increases again, leading to a progressive decrease in the rate of production of debris and sediments and hence availability of eroded material from the source region. At this point water discharge will prevail over sediment supply, leading to incision (low Q_s/Q_w-ratio). At the transition to warm and arid interglacial phases, sediment production rates in the source region will increase (high Q_s/Q_w-ratio). This will be followed by sediment transport to the basin and alluvial fan accumulation (high to balanced Q_s/Q_w-ratio), favoured by an increase in precipitation with the onset of the subsequent glacial period, until incision follows toward the end of the same glacial period, when the sediment transport capacity will prevail over sediment supply (low Q_s/Q_w-ratio).

The comparison of my OSL ages provides in general a good match with climatic proxies and indicates phases of enhanced incision towards the end of cold/wet phases and deposition during warm/dry periods and the early wetter stages, until discharge will prevail over sediment supply and alluvial fan incision will start again. Similar observations were made by Tofelde et al. (2017), who observed a 100yr cycle pattern of incision and deposition associated with fluvial activity and terrace formation. The data of my study suggest in turn a ca. 70 ka cycle, which is interrupted by the deposition of fan generation 3. Thus, I would not claim a constant cyclicity for the study area due to the limited amount of data available.

6. Conclusion

Twelve OSL samples from five sampling locations and nine samples from a depth profile for cosmogenic radionuclide dating were collected in the Santa Maria Valley in NW Argentina for alluvial fan dating. The results of the OSL (IRSL, respectively) measurements range from 0.4 ± 0.1 ka up to 271.8 ± 24.5 ka. Combined, my dating results, field mapping and stratigraphic observations allow differentiating 7 (/8) generations of alluvial fan deposits within the study area. The influence of neotectonic deformation on fan occurrence is assumed to have rather minor effects. A strong link on fan deposition, however, is observed in connection to climate variability linked to global glaciation cycles. Specifically, phases of incision correlate with high water discharge and possibly a low amount of sediment input (low Q_s/Q_w) associated with the termination of glacial phases (cold and wetter conditions). Conversely, alluvial fan deposition seems to have started during the transition to interglacial phases (high Q_s/Q_w-ratio). I suggest that deposition was triggered by an increase in availability of eroded material following a decrease in vegetation cover during arid interglacial phases, while incision was caused by an increase in river discharge during wetter phases (glacial periods), which led to a decrease in sediment supply, possibly in association with an increase in vegetation cover. To get a better picture of the relation in between depositional patterns of alluvial sediments and the impact of local tectonic structures as well as regional climatic patterns, further support by dating as well as an accurate study of underlying lithologies and tectonic structures, is needed.

Acknowledgements

I want to thank Prof. Manfred Strecker and Dr. Paolo Ballato for their support in financing the field campaign and sample processing as well as for the supervision of this thesis. Furthermore I want to thank Leonardo Escalante and Sara Figueroa for their support during field work as well as the provision of additional information based on their own study area. I want to thank Alexander Fülling of the Humboldt University Berlin for the help in carrying out the OSL/IRSL laboratory processing and Dr. Georg Schettler from the GeoForschungsZentrum Potsdam for the supervision during the gamma spectrometrical measurements. I want to thank Dr. Paolo Ballato, Sophie Boven, Adrian Jablanovski, Gregor Lauer-Dünkelberg and Heiko Pingel for enlightening discussions and/or detailed and constructive revisions to improve the manuscript. Last but not least I want to thank the firefighters of Cafayate for saving our lives when we got stuck in a canyon during the field campaign.

References

Allmendinger, R. W., Ramos, V. A., Jordan, T. E., Palma, M., & Isacks, B. L. (1983). Paleogeography and Andean structural geometry, northwest Argentina. *Tectonics*, *2*(1), 1-16.

Allmendinger, R. W., Jordan, T. E., Kay, S. M., & Isacks, B. L. (1997). The evolution of the Altiplano-Puna plateau of the Central Andes. *Annual review of earth and planetary sciences*, *25*(1), 139-174.

Baker, P. A., & Fritz, S. C. (2015). Nature and causes of Quaternary climate variation of tropical South America. *Quaternary Science Reviews*, *124*, 31-47.

Blair, T. C., & McPherson, J. G. (1994). Alluvial fan processes and forms. In *Geomorphology of desert environments* (pp. 354-402). Springer, Dordrecht.

Blair, T. C., & McPherson, J. G. (2009). Processes and forms of alluvial fans. In *Geomorphology of desert environments* (pp. 413-467). Springer, Dordrecht.

Bookhagen, B., Haselton, K., & Trauth, M. H. (2001). Hydrological modelling of a Pleistocene landslide-dammed lake in the Santa Maria Basin, NW Argentina. *Palaeogeography, Palaeoclimatology, Palaeoecology*, *169*(1-2), 113-127.

Bookhagen, B., & Strecker, M. R. (2012). Spatiotemporal trends in erosion rates across a pronounced rainfall gradient: Examples from the southern Central Andes. *Earth and Planetary Science Letters*, *327*, 97-110.

Bull, W. B. (1977). The alluvial-fan environment. *Progress in physical geography*, *1*(2), 222-270.

Burbank, D. W., & Anderson, R. S. (2001). *Tectonic geomorphology*. John Wiley & Sons., 4. Edition, 2005.

Buylaert, J. P., Murray, A. S., Thomsen, K. J., & Jain, M. (2009). Testing the potential of an elevated temperature IRSL signal from K-feldspar. *Radiation Measurements*, *44*(5-6), 560-565.

Dadson, S. J., Hovius, N., Chen, H., Dade, W. B., Hsieh, M. L., Willett, S. D., Hu, J.-C., Horng, M.-J., Chen, M.-C., Stark, C. P., Lague, D. & Lin, J.-C. (2003). Links between erosion, runoff variability and seismicity in the Taiwan orogen. *Nature*, *426*(6967), 648.

Dey, S., Thiede, R. C., Schildgen, T. F., Wittmann, H., Bookhagen, B., Scherler, D., Jain, V. & Strecker, M. R. (2016). Climate driven sediment aggradation and incision since the late Pleistocene in the NW Himalaya, India. *Earth and Planetary Science Letters, 449*, 321-331.

Dunai, T. J. (2010). *Cosmogenic nuclides: principles, concepts and applications in the earth surface sciences*. Cambridge University Press.

Fiorella, R. P., Poulsen, C. J., Pillco Zolá, R. S., Barnes, J. B., Tabor, C. R., & Ehlers, T. A. (2015). Spatiotemporal variability of modern precipitation δ18O in the central Andes and implications for paleoclimate and paleoaltimetry estimates. *Journal of Geophysical Research: Atmospheres*, *120*(10), 4630-4656.

Gosse, J. C., & Phillips, F. M. (2001). Terrestrial in situ cosmogenic nuclides: theory and application. *Quaternary Science Reviews*, *20*(14), 1475-1560.

Granger, D. E., & Muzikar, P. F. (2001). Dating sediment burial with in situ-produced cosmogenic nuclides: theory, techniques, and limitations. *Earth and Planetary Science Letters*, *188*(1-2), 269-281.

Hain, M. P., Strecker, M. R., Bookhagen, B., Alonso, R. N., Pingel, H., & Schmitt, A. K. (2011). Neogene to Quaternary broken foreland formation and sedimentation dynamics in the Andes of NW Argentina (25 S). *Tectonics*, *30*(2).

Haselton, K., Hilley, G., & Strecker, M. R. (2002). Average Pleistocene climatic patterns in the southern central Andes: Controls on mountain glaciation and paleoclimate implications. *The Journal of geology*, *110*(2), 211-226.

Hermanns, R. L., & Strecker, M. R. (1999). Structural and lithological controls on large Quaternary rock avalanches (sturzstroms) in arid northwestern Argentina. *Geological Society of America Bulletin*, *111*(6), 934-948.

Hermanns, R. L., Niedermann, S., Ivy-Ochs, S., & Kubik, P. W. (2004). Rock avalanching into a landslide-dammed lake causing multiple dam failure in Las Conchas valley (NW Argentina)—evidence from surface exposure dating and stratigraphic analyses. *Landslides*, *1*(2), 113-122.

Hermanns, R. L., Niedermann, S., Villanueva Garcia, A., & Schellenberger, A. (2006). Rock avalanching in the NW Argentine Andes as a result of complex interactions of lithologic, structural and topographic boundary conditions, climate change and active tectonics. *Massive rock slope failure: new models for hazard assessment. Kluwer, Dodrecht*.

Hilley, G. E., & Strecker, M. R. (2005). Processes of oscillatory basin filling and excavation in a tectonically active orogen: Quebrada del Toro Basin, NW Argentina. *Geological Society of America Bulletin*, *117*(7-8), 887-901.

Hodges, K. V. (2000). Tectonics of the Himalaya and southern Tibet from two perspectives. *Geological Society of America Bulletin*, *112*(3), 324-350.

Jordán, T. E., Isacks, B. L., Allmendinger, R. W., Brewer, J. A., Ramos, V. A., & Ando, C. J. (1983). Andean tectonics related to geometry of subducted Nazca plate. *Geological Society of America Bulletin*, *94*(3), 341-361.

Jordan, T. E., Nester, P. L., Blanco, N., Hoke, G. D., Dávila, F., & Tomlinson, A. J. (2010). Uplift of the Altiplano-Puna plateau: A view from the west. *Tectonics*, *29*(5).

Kleinert, K., & Strecker, M. R. (2001). Climate change in response to orographic barrier uplift: Paleosol and stable isotope evidence from the late Neogene Santa Maria basin, northwestern Argentina. *Geological Society of America Bulletin*, *113*(6), 728-742.

Mahan, S. (2015). U.S. Geological Survey Luminescence Dating Laboratory Optically Stimulated Luminescence (OSL) Sampling Instructions. *U.S. Department of the Interior U.S. Geological Survey, Information Handout.*

Marquillas, R. A., Del Papa, C., & Sabino, I. F. (2005). Sedimentary aspects and paleoenvironmental evolution of a rift basin: Salta Group (Cretaceous–Paleogene), northwestern Argentina. *International Journal of Earth Sciences*, *94*(1), 94-113.

McQuarrie, N., Horton, B. K., Zandt, G., Beck, S., & DeCelles, P. G. (2005). Lithospheric evolution of the Andean fold–thrust belt, Bolivia, and the origin of the central Andean plateau. *Tectonophysics*, *399*(1-4), 15-37.

Millar, R. J., Fuglestvedt, J. S., Friedlingstein, P., Rogelj, J., Grubb, M. J., Matthews, H. D., Skeie, B. S., Forster, P. M., Frame, D. J. & Allen, M. R. (2017). Emission budgets and pathways consistent with limiting warming to 1.5 C. *Nature Geoscience*, *10*(10), 741.

Molnar, P., & England, P. (1990). Late Cenozoic uplift of mountain ranges and global climate change: chicken or egg?. *Nature*, *346*(6279), 29-34.

Montgomery, D. R., Balco, G., & Willett, S. D. (2001). Climate, tectonics, and the morphology of the Andes. *Geology*, *29*(7), 579-582.

Murray, A. S., & Wintle, A. G. (2000). Luminescence dating of quartz using an improved single-aliquot regenerative-dose protocol. *Radiation measurements*, *32*(1), 57-73.

Murray, A. S., & Wintle, A. G. (2003). The single aliquot regenerative dose protocol: potential for improvements in reliability. *Radiation measurements*, *37*(4-5), 377-381.

Nelson, M. S., Gray, H. J., Johnson, J. A., Rittenour, T. M., Feathers, J. K., & Mahan, S. A. (2015). User guide for luminescence sampling in archaeological and geological contexts. *Advances in Archaeological Practice*, *3*(2), 166-177.

Pingel, H., Mulch, A., Alonso, R. N., Cottle, J., Hynek, S. A., Poletti, J., Rohrmann, A., Schmitt, A. K., Stockli, D. F. & Strecker, M. R. (2016). Surface uplift and convective rainfall along the southern Central Andes (Angastaco Basin, NW Argentina). *Earth and Planetary Science Letters*, *440*, 33-42.

Rhodes, E. J. (2011). Optically stimulated luminescence dating of sediments over the past 200,000 years. *Annual Review of Earth and Planetary Sciences*, *39*, 461-488.

Sobel, E. R., Hilley, G. E., & Strecker, M. R. (2003). Formation of internally drained contractional basins by aridity-limited bedrock incision. *Journal of Geophysical Research: Solid Earth*, *108*(B7).

Sobel, E. R., & Strecker, M. R. (2003). Uplift, exhumation and precipitation: tectonic and climatic control of Late Cenozoic landscape evolution in the northern Sierras Pampeanas, Argentina. *Basin Research*, *15*(4), 431-451.

Strecker, M. R., Alonso, R. N., Bookhagen, B., Carrapa, B., Hilley, G. E., Sobel, E. R., & Trauth, M. H. (2007). Tectonics and climate of the southern central Andes. *Annu. Rev. Earth Planet. Sci.*, *35*, 747-787.

Strecker, M. R., Cerveny, P., Bloom, A. L., & Malizia, D. (1989). Late Cenozoic tectonism and landscape development in the foreland of the Andes: Northern Sierras Pampeanas (26–28 S), Argentina. *Tectonics*, *8*(3), 517-534.

Strecker, M. R., Hilley, G. E., Bookhagen, B., & Sobel, E. R. (2011). Structural, geomorphic, and depositional characteristics of contiguous and broken foreland basins: examples from the eastern flanks of the central Andes in Bolivia and NW Argentina. *Tectonics of Sedimentary Basins: Recent Advances*, 506-521.

Thiede, R. C., Arrowsmith, J. R., Bookhagen, B., McWilliams, M. O., Sobel, E. R., & Strecker, M. R. (2005). From tectonically to erosionally controlled development of the Himalayan orogen. *Geology*, *33*(8), 689-692.

Trauth, M. H., & Strecker, M. R. (1999). Formation of landslide-dammed lakes during a wet period between 40,000 and 25,000 yr BP in northwestern Argentina. *Palaeogeography, Palaeoclimatology, Palaeoecology*, *153*(1-4), 277-287.

Wagner, G. A., Greilich, S., & Kadereit, A. (2003). Kaltes Leuchten erhellt die Vergangenheit: Lumineszenzdatierung. *Physik in unserer Zeit*, *34*(4), 160-166.

Wallinga, J., S. Murray, A., & Bøtter-Jensen, L. (2002). Measurement of the dose in quartz in the presence of feldspar contamination. *Radiation Protection Dosimetry*, *101*(1-4), 367-370.

Whipple, K. X. (2009). The influence of climate on the tectonic evolution of mountain belts. *Nature geoscience*, *2*(2), 97.

Whipple, K. X., & Meade, B. J. (2006). Orogen response to changes in climatic and tectonic forcing. *Earth and Planetary Science Letters*, *243*(1-2), 218-228.

Willett, S. D. (1999). Orogeny and orography: The effects of erosion on the structure of mountain belts. *Journal of Geophysical Research: Solid Earth*, *104*(B12), 28957-28981.

Wintle, A. G., & Murray, A. S. (2006). A review of quartz optically stimulated luminescence characteristics and their relevance in single-aliquot regeneration dating protocols. *Radiation measurements*, *41*(4), 369-391.

Appendix

Tables

Table 2 *– Shielding measurements for sampling site 7 / cosmogenic nuclide dating (CCA-16-03).*

Azimuth	Angle (°)	Azimuth	Angle (°)
2	2	160	11
6	5	162	10
15	4	164	9
18	0	165	9
21	0	167	9
22	1	169	10
30	2	172	9
36	1	174	9
45	1	176	8
60	0	178	7
63	0	179	6
65	0	180	5
73	5	185	5
85	8	187	3
86	7	188	3
87	9	191	3
89	11	220	0
95	12	225	2
98	11	230	4
100	10	232	3
108	13	237	3
109	12	245	4
111	12	250	4
114	13	265	4
126	10	267	3
128	11	271	3
131	10	285	3
135	12	306	3
137	14	311	4
146	13	314	4
147	14	316	3
149	14	325	3
150	12	335	3
151	14	340	4
154	15	344	3
157	12	354	2

Graphics

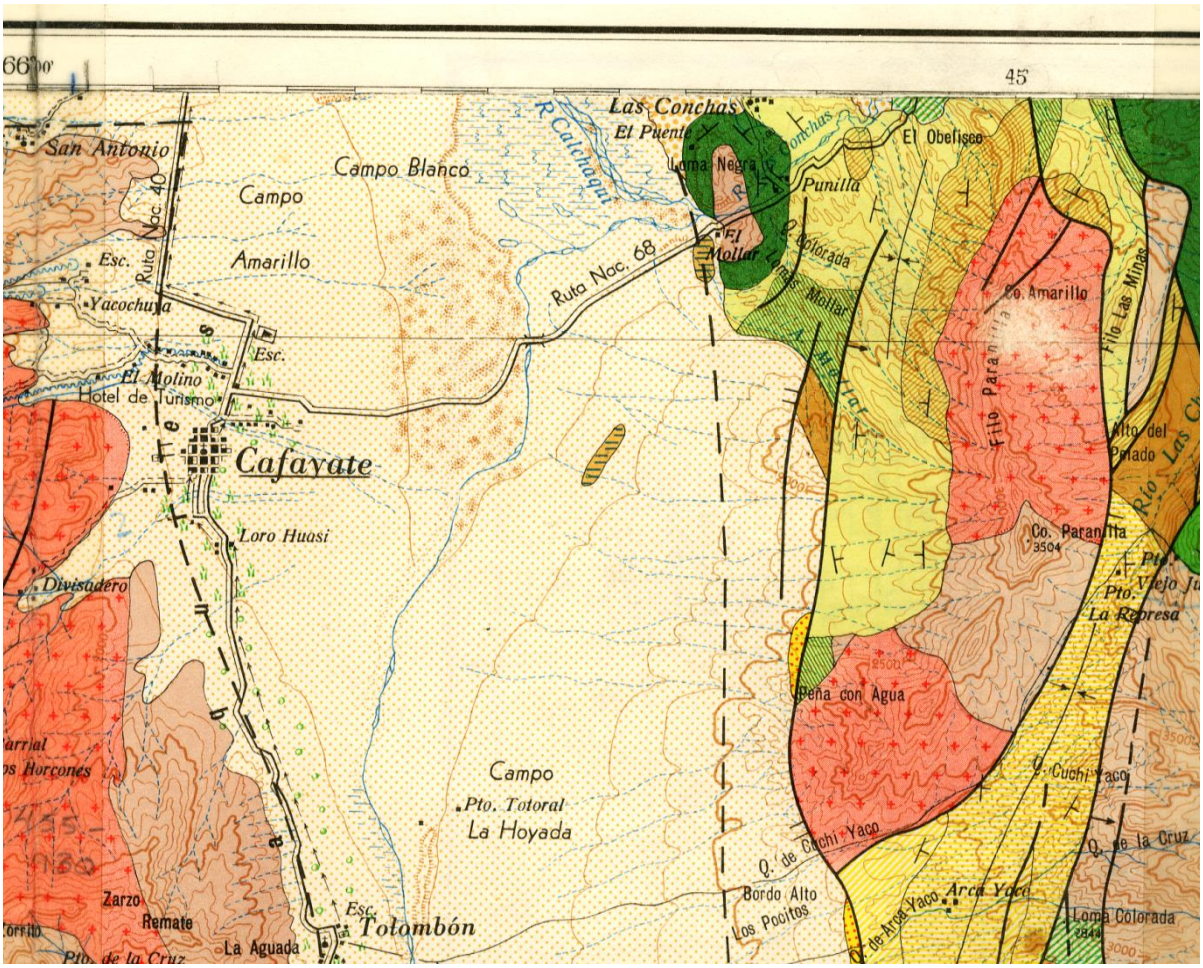

Figure 22 – Extraction of a scanned Geologic map of the valley around the study area, Scale 1:200000. The stratigraphic compartmentalisation of the Filo Paranilla into two granitic sections and one metamorph portion is visible as well as the Loma Negra in the north-west of it, divided by the rute No. 68 coming from the city of Cafayate.

(Map 10e, Cafayate, Provincias de Tucuman, Salta y Catamarca; Version No.177, 1980; Edit.: Ministerio de economía, Secretaría de estado de minería, Subsecretaría Técnica, Servicio Geológico Nacional, Departamento Cartas Geológicas)

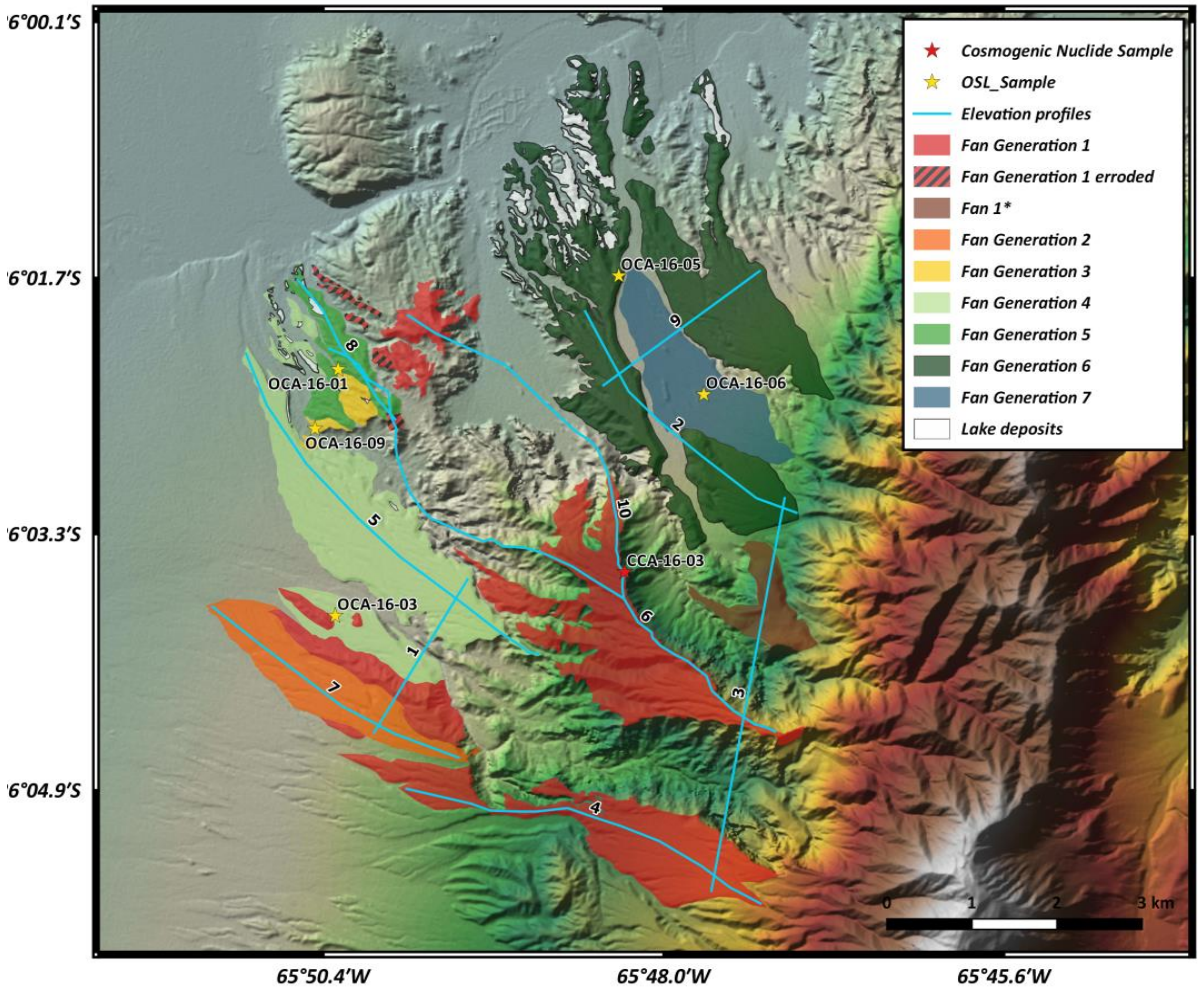

Figure 23 – Overview of several topographic profiles along and orthogonal to the fan generations used for fan interpretation.

1)

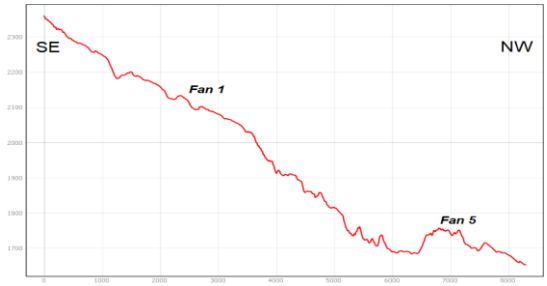

6)

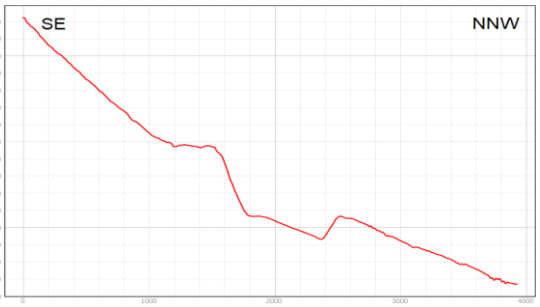

2)

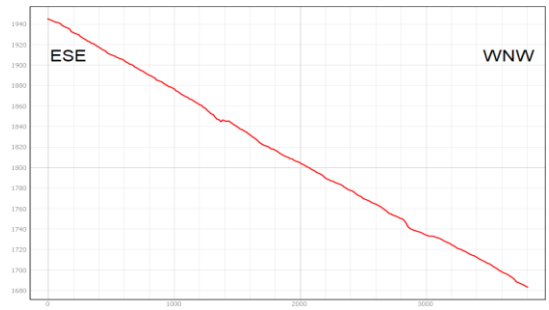

7)

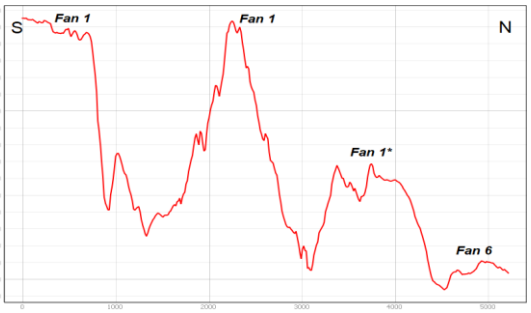

3)

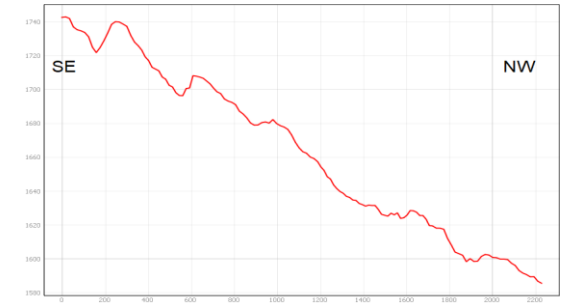

8)

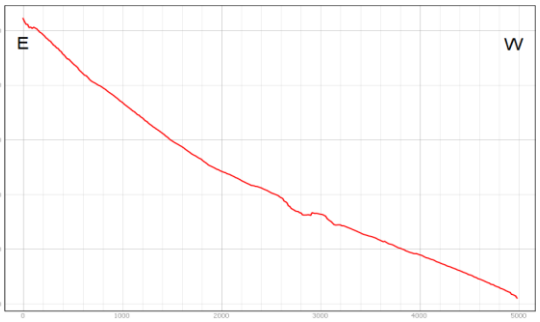

4)

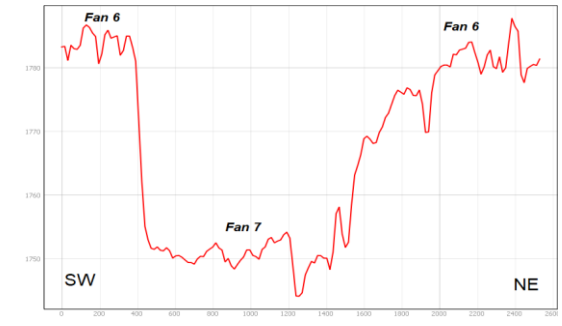

9)

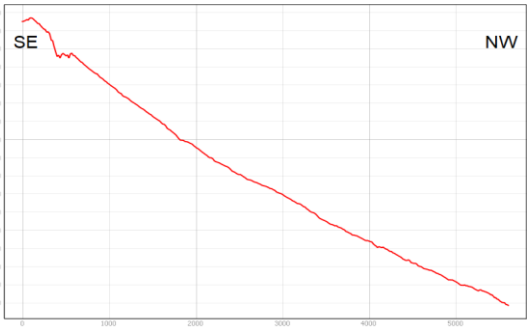

5)

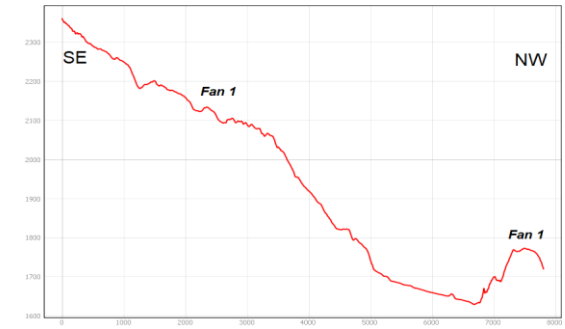

10)

Figure 24 – Profiles 1-10 as shown in the map in figure 23.